European Journal of Medicinal Chemistry 237 (2022) 114396

Contents lists available at ScienceDirect

European Journal of Medicinal Chemistry

journal homepage: www.elsevier.com/locate/ejmech

New salicylic acid derivatives, double inhibitors of glycolate oxidase and lactate dehydrogenase, as effective agents decreasing oxalate production

Maria Dolores Moya-Garzon [a,1], Barbara Rodriguez-Rodriguez [b], Cristina Martin-Higueras [b], Francisco Franco-Montalban [a], Miguel X. Fernandes [b,2], Jose A. Gomez-Vidal [a], Angel L. Pey [c], Eduardo Salido [b,**], Monica Diaz-Gavilan [a,*]

[a] Departamento de Química Farmacéutica y Orgánica, Facultad de Farmacia, Campus de Cartuja S/n, 18071, Granada, Spain
[b] Departamento de Ciencias Médicas Básicas, Facultad de Medicina, Universidad de La Laguna, Instituto de Tecnologías Biomédicas (ITB), Centro de Investigación Biomédica en Red de Enfermedades Raras (CIBERER), Tenerife, Spain
[c] Departamento de Química Física, Unidad de Excelencia en Química Aplicada a Biomedicina y Medioambiente e Instituto de Biotecnología, Universidad de Granada, Av. Fuentenueva S/n, 18071, Granada, Spain

ARTICLE INFO

Keywords:
Hyperoxaluria
Salicylic acid
Glycolate oxidase
Lactate dehydrogenase
Oxalate
Glyoxylate

ABSTRACT

The synthesis and biological evaluation of double glycolate oxidase/lactate dehydrogenase inhibitors containing a salicylic acid moiety is described. The target compounds are obtained in an easily scalable two-step synthetic procedure. These compounds showed low micromolar IC_{50} values against the two key enzymes in the metabolism of glyoxylate. Mechanistically they behave as noncompetitive inhibitors against both enzymes and this fact is supported by docking studies. The biological evaluation also includes *in vitro* and *in vivo* assays in hyperoxaluric mice. The compounds are active against the three types of primary hyperoxalurias. Also, possible causes of adverse effects, such as cyclooxygenase inhibition or renal toxicity, have been studied and discarded. Altogether, this makes this chemotype with drug-like structure a good candidate for the treatment of primary hyperoxalurias.

1. Introduction

Recent investigations on salicylic acid (SA) derivatives have unveiled their capacity to decrease the production of oxalate in mouse primary hepatocytes with primary hyperoxaluria type 1 (PH1) (*Agxt1*$^{-/-}$ hepatocytes) [1]. This important finding means their possible utility in oxalate accumulation diseases. Salicylates' activity appears to be to some extent related to inhibition of the enzyme glycolate oxidase (GO) [1]. This enzyme generates glyoxylate, a highly reactive metabolite that the enzyme alanine-glyoxylate aminotransferase (AGT) clears away. However, PH1 patients present a defective AGT. This leads to an accumulation of glyoxylate that undergoes oxidation to oxalate by the hepatic lactate dehydrogenase (LDHA). Oxalate is excreted in urine. If its production is excessive, oxalate binds calcium to form crystals that produce kidney damage and subsequent accumulation of oxalate in different tissues, compromising the life of patients [2]. GO inhibition is a strategy

Abbreviations: ACN, acetonitrile; AGT, alanine-glyoxylate aminotransferase; CaOx, calcium oxalate; COX, cyclooxygenase; CPA, 2-chloro-*N*-(3,5-dihydroxyphenyl)acetamide; DCE, 1,2-dichloroethane; DCM, dichloromethane; DMAB, 3-(dimethylamino)benzoic acid; DMSO, dimethylsulfoxide; EC, effective concentration; EMA, European Medicine Agency; FDA, Food and Drug Administration; GALS, genetic algorithm local search; GO, glycolate oxidase; GOi, glycolate oxidase inhibitor; HRMS, high resolution mass spectrometry; IC, inhibitory concentration; LCMS, liquid chromatography mass spectrometry; LDH, lactate dehydrogenase; LDHi, lactate hydrogenase inhibitor; mp, melting point; MBTH, 3-methyl-2-benzothiazolinone hydrazine; MTT, 3-(4,5-dimethylthiazol-2-yl)-2,5-diphenyltetrazolium bromide; NMR, nuclear magnetic resonance; PH, primary hyperoxaluria; RMSD, root-mean square deviation; RO, relative oxalate; rt, room temperature; SA, salicylic acid; SRT, substrate reduction therapy; TLC, thin layer chromatography.

* Corresponding author.
** Corresponding author.
E-mail addresses: esalido@ull.edu.es (E. Salido), monicadg@ugr.es (M. Diaz-Gavilan).
[1] Present address: Department of Pathology, Stanford University School of Medicine, Stanford 94305, CA, USA and Stanford ChEM-H, Stanford University, Stanford 94305, CA, USA.
[2] Present address: Instituto Universitario de Bio-Orgánica "Antonio González" (IUBO-AG), C/Astrofísico Francisco Sánchez 2, Universidad de La Laguna, 38200 La Laguna, Tenerife, Spain.

https://doi.org/10.1016/j.ejmech.2022.114396
Received 13 September 2021; Received in revised form 2 April 2022; Accepted 13 April 2022
Available online 25 April 2022

for substrate reduction therapy (SRT) in PH1, whose efficiency and safety has been proved in *Agxt1*$^{-/-}$ mice [3]. Other PHs are due to genetic defects in the glyoxylate reductase-hydroxypyruvate reductase (GRHPR) (PH2) [4] and in the 4-hydroxy-2-oxoglutarate aldolase (HOGA) (PH3) [5] enzymes. Although these are considered less severe forms of hyperoxaluria, recent investigations have revealed that their severity is more important than previously believed [6–10]. Common to all hyperoxalurias is the overproduction of oxalate synthesized from glyoxylate by LDHA and the ongoing efforts to develop a suitable pharmacological treatment [11–18]. Only very recently, the FDA and the EMA agencies have approved the first pharmacological treatment for PH1, lumasiran [19,20]. This one is a RNA*i* drug against GO administered by subcutaneous injection [21,22].

Compound **1** [1] is a GO inhibitor (GOi) similar in potency against recombinant mouse GO (*m*GO) to CCPST [3], a known noncompetitive GOi (Fig. 1). However, **1** is significantly more potent than CCPST decreasing oxalate production in *Agxt1*$^{-/-}$ mouse hepatocytes (*in vitro*) (see IC_{50} *vs* EC_{50}, Fig. 1). This raised questions about the biological mechanism of **1** and the possible existence of an alternative, cooperative target [1]. Since compound **1** was designed as a substrate analogue for GO, and considering that GO and LDH can both use glyoxylate as a substrate and catalyse its oxidation, the most straightforward candidate for a possible off-target of **1** is LDHA. Also, RNA*i*-mediated silencing of LDH has been recently proved to be an efficient strategy against the production of oxalate and kidney damage by calcium oxalate (CaOx) in animal models of PH1 and PH2 [23,24]. A clinical trial is currently evaluating nedosiran, an RNA*i* drug against LDHA, for the treatment of PHs [25]. Moreover, stiripentol, an LDH inhibitor (LDHi) clinically used as antiepileptic, has shown urinary oxalate decreasing activity in a human PH1 patient [26–28]. The *m*-(2-furyl)benzoic moiety, present in **1**, is in fact contained in previously described LDHAi's [29]. There are five different tetramer LDH isozymes, with different tissue distribution, formed by combinations of two subunits, M (muscle) and H (heart). Liver isozyme, LDHA, is also present in skeletal muscle, and it is formed by four M subunits; cardiac isozyme, LDHB, is formed by four H subunits [30,31].

Double GO/LDHAi's could present several advantages in therapy against PHs, targeting two key enzymes involved in the same metabolic route towards oxalate production. Moreover, small drugs present the advantage of possible oral administration in contrast to RNA*i* drugs. Thus, as a rational progress of our research, we focused on the design of novel SA derivatives as promising drug-like compounds, substrate analogues for GO and LDH. Recently, dual GO/LDHAi's have been reported as hybrid molecules designed by linkage of a known GOi and a known LDHi [32]. Differently, our approach aims at targeting both enzymes using the same SA head that includes both pharmacophore moieties. This way, the resulting molecules present lower molecular weight than hybrids, a characteristic that should help pharmacokinetics. This is especially desirable as the two target enzymes are located in different intracellular compartments. Our former docking predictions for **1** [1] suggested the formyl group establishes no binding interaction to human GO (*h*GO). Not being essential for the biological activity, the formyl substituent offers a modulation point to obtain structurally diverse analogues. Docking **1** inside *h*GO and *h*LDHA we found that its salicylic head can indeed fit both enzymes. It is also easily envisioned that elongated derivatives of **1** might present reinforced binding by reaching the hydrophobic channel [33] and the hydrophobic cleft, that give access to the catalytic sites of *h*GO and *h*LDHA, respectively. In addition, introducing some degree of flexibility in the molecules, might allow the accommodation to the particular structure of each enzyme. Sticking to our preference of using simple, economic and easily scalable synthetic procedures to facilitate an eventual industrial development, we have prepared a family of SAs, structural derivatives of **1**, our lead compound with the best phenotypic activity in cell culture. The new derivatives contain hydrophobic side chains separated from the SA head by a flexible 5-aminomethyl-2-furyl linker. The linker allows rotational freedom and includes an amino group to reinforce the interaction with the enzymes by hydrogen donation/acceptance. Herein we present the two-step-synthesis of aminomethylfuryl SAs with improved enzymatic and phenotypic activity in PH1, PH2 and PH3 mouse models.

2. Results and discussion

2.1. Chemical synthesis

We designed the final molecules including hydrophobic, aromatic or aliphatic amino side chains with different bulkiness and electronic characteristics. In a first synthetic step, compound **1** was prepared by Suzuki coupling between methyl 5-iodosalicylate and 5-formyl-2-furanboronic acid [1]. The second reaction yielded the aminomethylfuryl SAs (**2**) by reductive amination between **1** and primary or secondary amines (**3**), including substituted anilines (**3a-e**), benzyl amines (**3f-j**), piperidine (**3k**) and propargyl amine (**3l**) (Scheme 1). Thus, we classify the final compounds type **2** as aromatic amines (anilines) (**2a-e**) and aliphatic amines (**2f-l**). All of them are secondary amines except for **2k**, with tertiary nitrogen. Flat aromatic fragments with different electronic densities and aliphatic moieties were explored (R^1).

Upon soft heating, secondary amines type **2** polymerize to the blue

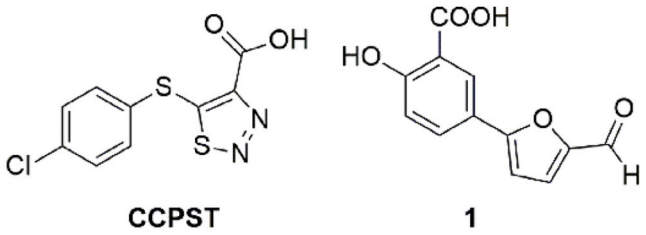

	CCPST	1
Recombinant *m*GO IC_{50} (μM)	43.5	38.2
Mouse hepatocytes *Agxt1*$^{-/-}$ EC_{50} (μM)	25.3	3.5

Fig. 1. Structure and activities of glycolate oxidase inhibitors CCPST and **1**. Inhibition of isolated recombinant mouse enzyme (IC_{50}) and decrease of oxalate production in *Agxt1*$^{-/-}$ mouse hepatocytes (EC_{50}) (*in vitro*) [1].

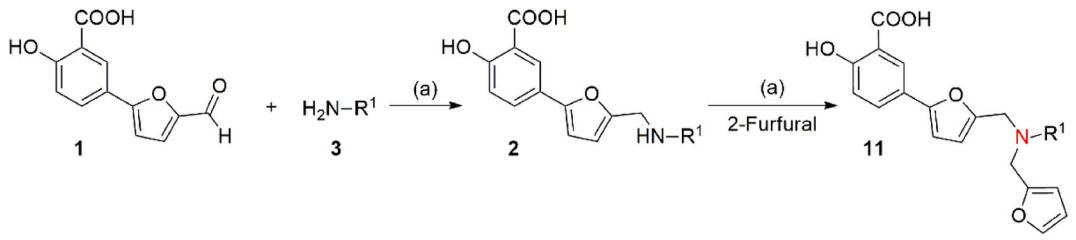

Compound	R^1	Compound	R^1
2a[a]	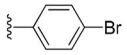	**2h**[a]	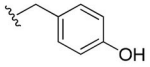
2b[a]	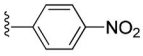	**2i**[a]	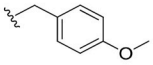
2c[b]	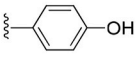	**2j**[a]	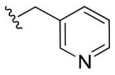
2d[b]	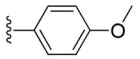	**2k**	
2e[a]	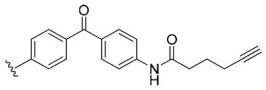	**2l**[a]	
2f[a]	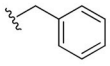	**11**	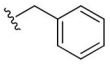
2g[a]	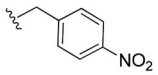		

Scheme 1. Preparation of aminomethylfuryl salicylic acids. Reaction conditions: (a) i) MeOH/DCM 3/1, molecular sieves (3 Å), room temperature, darkness; ii) $NaBH(OAc)_3$, room temperature; iii) H_2O, 0 °C. [a]Isolated as ammonium salicylates (ammonium counter ion gained during the purification process). [b]Not isolated because of instability issues.

coloured difurylmethane **4** (Scheme 2). Acidic medium also helps this polymerization even at low temperatures. This polymerization is responsible for the low yields observed for **2a, 2b** and **2e** and for the failure to isolate pure **2c** and **2d**. Acid-catalyzed polymerization of 2-furylcarbinols (**5**, Scheme 2) to di-(2-furyl)methanes is a well-known process [34–36]. It has been explained *via* etherification [37] between two molecules of **5** (steps a-c) and further decomposition of the resulting ether (**6**) into formaldehyde (**7**) and the final difurylmethane (step d) [38]. One reference was found regarding polymerization of 2-furylmethanamines to di-(2-furyl)methanes [39]. The mechanism was explained matching the same ether intermediate (**6**), which would be formed by water addition to the cation **8** (step e). Intermediate **8** would be obtained after protonation and elimination of the amino fragment in **2** (steps a-b). Symmetric tertiary amines **9f** and **9l** (Scheme 2) were isolated as secondary products in the reactions between **1** and the amines **3f** and **3l**. The tertiary amines can be products of a second reductive amination happening after **2f** and **2l** formation. However, **9f** and **9l** also formed during the chromatographic purification on acidic silica gel. Thus, we suggest that amines type **9** could be precursors of **4**, meaning that **4** could also be formed from secondary amines type **2** by a similar mechanism as the one described for furylcarbinols (Scheme 2, steps a-d), without needing addition of water (step e). The last step of this process would involve the elimination of the imine derivative **10**, which would decompose delivering the starting amine type **3**. In fact, these amines were also isolated during the chromatographic purification. In our SA derivatives, the cation **8** would be additionally stabilized by the phenol functionality [39].

The tertiary amines **9f** and **9l** were included for biological evaluation. In addition, compound **11** (Scheme 1) was prepared as a simplified analogue of **9f**, to assess the relation between structure and activity in these branched derivatives. Compound **11** was prepared from **2f** by reductive amination using 2-furfural (Scheme 1).

2.2. Biological evaluation against recombinant enzymes

The final compounds were evaluated against recombinant enzymes *m*GO, *h*GO, *h*LDHA and *h*LDHB. Initially, a screening of inhibition percentages was made on GO and LDH at 20 μM and 10 μM doses, respectively, to discard low potency molecules. For the best hits we also determined IC_{50}, K_i and inhibition mechanism.

2.2.1. Inhibition of GO

The compounds were initially evaluated following a colorimetric method with a coupled HRP reaction using the hydrogen peroxide produced by GO [1,3]. However, we found that some of the tested compounds interfered in this evaluation method (Supporting *Information*, Table S1). Even though this colorimetric protocol did not enable us to reliably determine the activity of the compounds, it allowed us to discard the low potency compounds **2f-k**, with inhibition percentages below 50% at 20 μM (Supporting *Information*, Table S2). Alternatively, we optimized an end-point assay using the fluorogenic reagent Amplex® Red and a HRP coupled reaction to determine inhibition percentages (Supporting *Information*, Table S3) and IC_{50}s (Table 1) for the rest of the compounds.

The new aminomethylfuryl SAs resulted up to 18 times more potent against GO isozymes than the lead compound **1** (Table 1). The best

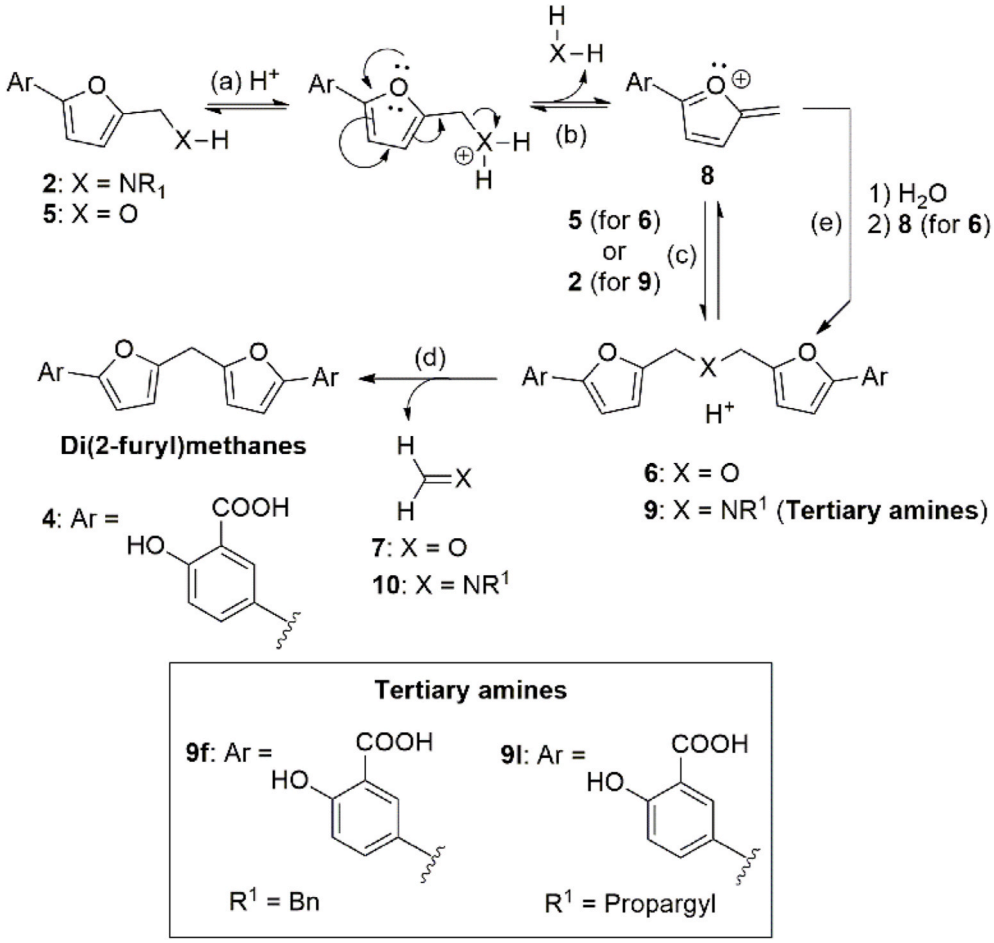

Scheme 2. Mechanisms for the formation of difurylmethanes and tertiary amines from 2-furylcarbinols and 2-furylmethanamines.

Table 1
Values of IC_{50} (μM) obtained for aminomethylfurylsalicylic acids on recombinant enzymes.

Compound	*m*GO[a]	*h*GO[a]	*h*LDHA[b]	*h*LDHB[b]
1	14.4 ± 1.4	28.2 ± 10.7	13.2 ± 1.5	29.0 ± 8.0
2a	3.1 ± 0.3	4.2 ± 0.2	0.6 ± 0.0	1.1 ± 0.2
2b	5.4 ± 0.1	10.3 ± 0.9	1.5 ± 0.3	5.9 ± 1.1
2e	1.3 ± 0.1	2.4 ± 0.1	0.5 ± 0.0	0.3 ± 0.01
2f	ND[c]	ND[c]	2.5 ± 0.5	3.3 ± 0.6
2g	ND[c]	ND[c]	8.0 ± 0.8	ND[d]
2l	8.1 ± 0.8	17.3 ± 3.5	2.0 ± 0.1	11.8 ± 1.0
9f	1.8 ± 0.1	1.5 ± 0.2	0.4 ± 0.2	0.2 ± 0.01
9l	0.8 ± 0.1	2.0 ± 0.1	1.6 ± 0.4	2.3 ± 0.3
11	8.0 ± 0.4	16.8 ± 1.0	2.3 ± 0.3	4.3 ± 1.0

[a] Mean of three/four replicates with eight concentrations of inhibitor each (enzyme concentration 25 nM; glycolate concentration 180 μM) ± SD.
[b] Mean of three/four replicates with eight concentrations of inhibitor each (enzyme concentration 0.0150 units/mL; pyruvate concentration 1 mM) ± SD.
[c] Not determined (ND) as the percentage inhibition at 20 μM was lower than 30%.
[d] Not determined as the percentage of inhibition at 10 μM was lower than 50%.

potencies were achieved by the bulkier **9f** and **9l** and the more elongated compound **2e**, with IC_{50} values below 2.5 μM against both isozymes. The tertiary aliphatic amines, **9f** and **9l**, present two salicylfuryl branches and a benzyl (**9f**) or propargyl (**9l**) one (Scheme 2). The removal of one salicylic ring of **9f** to give compound **11** produced a decrease in the inhibitory activity of the molecule on both isozymes. The secondary aniline **2e** is *para*-substituted with an electron withdrawing acyl group. Interestingly, other deactivated secondary anilines such as **2a** and **2b** resulted potent hits with IC_{50} values around 5 μM on both GO isozymes. Secondary anilines (**2a**, **2b**, **2e**) were more potent GOi's compared to secondary aliphatic amines (benzyl amines **2f**-**2j** and propargyl amine **2l**) (Tables 1 and S2). The tertiary aliphatic amine **2k** presented a marginal inhibitory activity (Table S2). In this last case, the three-dimensional conformation of the piperidine ring differs substantially from the flat shape of the aromatic rings. Compounds **2a**, **2b** and **2e**, as well as **9f** and **9l** include aromatic rings on the side chain attached to C5 of the furan ring. Compound **2l** lacks the aromatic moiety on the side chain but presents a flat π-system that could establish the same type of interactions as an aromatic ring.

2.2.2. *Inhibition of human lactate dehydrogenase A*

We used a kinetic fluorometric protocol based on the disappearance of NADH [29]. Any possible interference was neutralized by subtraction of the baseline reading. In general, those compounds presenting the best inhibitory activities on GO, happened to be also the most active ones on *h*LDHA (Table 1). The new aminomethylfuryl SAs resulted up to 30 times more potent *h*LDHAi's than the parent compound **1** (IC_{50} = 13 μM) (Table 1). Compounds **2a**, **2e** and **9f** show IC_{50} values against *h*LDHA below 1 μM, and **2b** and **9l** stay around 1.5 μM (Table 1). These are again deactivated secondary anilines and tertiary aliphatic amines. Once more, the removal of one salicylic head of **9f** to give compound **11** produced a decrease of the *h*LDHA inhibitory activity of the molecule. Noteworthy, secondary aliphatic amines **2f**, **2g**, and **2l** (benzyl amine, *p*-nitrobenzyl amine and propargyl amine), which were weak or modest GOi's, show IC_{50} values between 2 and 8 μM against *h*LDHA (Table 1). The satisfactory activities of **2f** and **2g** contrast with the poor one of **2j**

(3-pyridylmethyl amine), despite of being isosteres (**2f** and **2j**) or presenting deactivated benzyl fragments (**2g** and **2j**). This discourages the use of pyridine-based side chains. Secondary benzyl amines with electron-rich rings (**2h**, **2i**) failed to achieve good *h*LDHA inhibition with percentages between 18 and 30% at a concentration of 10 μM (data not shown).

Thus, building the structure of 5-furylSAs beyond the furan ring using a flexible two-atom aminomethyl linker improves the GO and LDHA inhibitory activity compared to the lead compound **1**. Flat side chains with π-systems appear to be the best option. The amine contained in the linker can be either a tertiary aliphatic one or a deactivated secondary aniline.

2.2.3. Inhibition of human lactate dehydrogenase B

We evaluated the activity of our compounds on *h*LDHB using the same kinetic fluorometric method based on NADH disappearance (Table 1). The most potent *h*LDHAi's, in terms of IC_{50}, resulted to be also the most potent *h*LDHBi's (Table 1).

2.3. Determination of inhibition kinetics

We chose representative compounds with the best inhibitory activities on *h*GO and *h*LDHA (**1**, no elongated side chain; **2a**, secondary aniline; **2l**, secondary aliphatic amine; **9f**, tertiary aliphatic amine). We found that these compounds behave as noncompetitive inhibitors of enzymes *m*GO, *h*GO and *h*LDHA, with α values higher than 1 against GO isozymes (mixed type noncompetitive) and, except for **2l**, equal to 1 against *h*LDHA [40].

2.3.1. Inhibition kinetics on glycolate oxidase

We used a fluorometric kinetic method based on the reagent Amplex® Red to determine the K_M value and the SAs mechanism of inhibition. We found K_M values for glycolate of 19 and 13 μM for *h*GO and *m*GO, respectively. Assays measuring the enzymatic activity in the presence of four different inhibitor concentrations and ten different substrate concentrations, showed a noncompetitive mixed type mechanism (α > 1) with respect to substrate glycolate. Non-linear "initial velocity (v_0) *vs* substrate concentration" plots showed decrease of V_{max} and increase of the apparent K_M with increasing concentrations of inhibitor and Lineweaver-Burk graphs showed intersection in the second quadrant for all compounds. The most potent compounds against *h*GO, the *p*-bromoaniline **2a** and the benzyl amine **9f**, presented K_i values of 1.1 and 2.3 μM, respectively (Table 2) (full data and graphs in Supporting *Information*, sections S10.1 and S10.2). The same determinations on *m*GO isozyme (compounds **1** and **2l**) resulted with the same mechanism of inhibition. However, it is worth highlighting that the presence of substrate influences more the binding of **1** and **2l** to *m*GO than to *h*GO, as α values are markedly higher for the mouse isozyme (Table 2) (full data and graphs in Supporting *Information*, section S10.3).

Compound **2l**, with a propargyl amine moiety, is susceptible to bind covalently to the flavin cofactor of GO (FMN) [41]. Thus, in order to determine whether **2l** is a reversible or irreversible *h*GOi, the recovery of the enzymatic activity in the presence of the inhibitor was measured in a "jump dilution" experiment [40,42]. Compounds **1** and **9f** were used as reversible controls. The progress curves obtained for the three compounds indicated that all of them behave as reversible inhibitors (full data and graphs in Supporting *Information*, section S11).

Table 2
Comparison of K_i and IC_{50} values obtained for selected salicylates on glycolate oxidase (noncompetitive mixed type inhibition).

Compound	*h*GO			*m*GO		
	IC_{50}	K_i	α	IC_{50}	K_i	α
1	28.2	18.2	9.5	14.4	7.9	15.3
2a	4.2	1.1	16.7	3.1	ND	ND
2l	17.3	24.7	5.2	8.1	10.5	11.1
9f	1.5	2.3	8.0	1.8	ND	ND

Units: μM. K_i calculated as the mean of two/three independent experiments with three replicates each one. ND: Not determined.

2.3.2. Inhibition kinetics on lactate dehydrogenase

We used the fluorometric kinetic method based on NADH to determine K_M and to study the SAs mechanism of inhibition on both LDH isozymes. We found K_M values for pyruvate of 176 and 44 μM for *h*LDHA and *h*LDHB, respectively, which closely agrees with bibliography [43]. Assays measuring the enzymatic activity of our compounds in the presence of four/five different inhibitor concentrations and nine/ten different substrate concentrations, showed a noncompetitive inhibition (α = 1) for the compounds **1**, **2a** and **9f** on *h*LDHA. Non-linear "initial velocity (v_0) *vs* substrate concentration" plots showed decrease of V_{max} and no effect on the K_M (with increasing concentrations of the inhibitor) and Lineweaver-Burk graphs showed intersection on the *x* axis. Only compound **2l** showed a more difficult-to-read behaviour with intersection in the second quadrant in the Lineweaver-Burk and a slight decrease of the apparent K_M, raising the chance of **2l** to be a mixed type inhibitor with a low α value (α = 4). However, for all compounds, statistical parameters are favourable to a pure noncompetitive inhibition. All the compounds resulted better *h*LDHAi's than *h*GOi's. The most potent compounds against *h*LDHA, are again the tertiary amine **9f**, with a K_i value in the two-digits nanomolar range (90 nM), followed by the deactivated *p*-bromoaniline **2a** with a K_i value slightly below 1 μM (Table 3) (full data and graphs in Supporting *Information*, sections S10.4 and S10.5). The same assays performed on *h*LDHB led to similar results regarding the mechanism of inhibition (full data in Supporting *Information*, section S10.6): noncompetitive inhibitors (**1** and **9f**) or mixed type inhibitors with low α value (**2l**) (α = 3) (Table S136). As it happened for *h*LDHA, the tertiary amine **9f** was again the most potent inhibitor on *h*LDHB. Compounds **1** and **9f** were the ones with the best selectivity for *h*LDHA, with an approximately 9-fold lower K_i on this isozyme *vs* *h*LDHB (Table 3).

In summary, inhibition kinetics studies on GO and *h*LDH suggest that salicylates exert their effect through noncompetitive (with substrate) mechanisms regardless of their bulkiness (linear or branched). Noncompetitive inhibition is not affected by the substrate concentration, which is an advantage *in vivo*. The next step in our research is determining the reason for this noncompetitive mechanism in molecules designed as substrate analogues. Site-directed inhibitors can exert a noncompetitive mechanism in certain situations [40,44], such as on isomechanism enzymes, enzymes with induced-fit inhibition mechanism or multi-substrate/multi product enzymes. Nothing has been described about the existence of isomechanism or induced-fit mechanisms in GO or LDHA. On the other hand, noncompetitive mechanisms could suggest an allosteric binding to the enzyme. Although there are precedents of noncompetitive GOi's, such as CCPST [3] or the flavonoid quercetin [45], nothing has been described about the existence of allosteric

Table 3
Comparison of K_i and IC_{50} values obtained for selected salicylates on lactate dehydrogenase isozymes.

Compound	*h*LDHA			*h*LDHB			$K_i(B)/K_i(A)$
	IC_{50}	K_i	α	IC_{50}	K_i	A	
1	13.2	1.4	1	29.0	12.9	1	9.2
2a	0.6	0.9	1	1.1	ND	–	ND
2l	2.0	6.1	1	11.8	5.1	1	0.8
2l	2.0	1.9	4	11.8	2.0	3	1.1
9f	0.4	0.09	1	0.2	0.7	1	8

Units: μM. Values of IC_{50} and K_i are calculated as the mean of three independent experiments. Values of α = 1 indicate noncompetitive inhibition; values of α > 1 indicate mixed type inhibition. For compound **2l**, parameters corresponding to noncompetitive and mixed type inhibition models are shown. ND: Not determined.

binding sites in GO. However, allosteric *h*LDHA [46] and *h*LDHB [47] inhibition has indeed been achieved. We have used docking to get preliminary data related to the binding site of our SAs (see Docking Results Sections below).

2.4. Biological evaluation in hyperoxaluric mouse hepatocytes: Oxalate determination

Simultaneously targeting two different enzymes related to the production of oxalate, should increase the efficiency of the treatment, and should lead to drugs with utility in the three types of PHs. The potential of the compounds to decrease oxalate production was tested on hyperoxaluric primary hepatocytes cultured from PH1, PH2 and PH3 mouse models (*Agxt1*$^{-/-}$ [48], *Grhpr*$^{-/-}$ [49] and *Hoga1*$^{-/-}$ [50], respectively). Primary hepatocytes were incubated in the presence of the inhibitor and challenged with glycolate (PH1 and PH2 models) or hydroxyproline (PH3 model). Oxalate in the extracellular medium was measured after 24 and 48 h from the administration of the inhibitor, using commercial colorimetric kits and providing relative oxalate (RO) data (Table 4). Cell viability through the assay was assessed by the MTS tetrazolium method; no evidence of cell death could be observed for any of the compounds at the concentration used in the oxalate assay (full data in Supporting *Information*, section S12).

We found that our compounds decreased oxalate output in the three types of PHs (Table 4). Remarkable activities in PH1, the most severe and prevalent PH, were found for **1**, **2a**, **2b**, **2f**, **2l** and **11**. Some of them (**1**, **2b**, **2l** and **11**) produced disappearance of oxalate in the extracellular medium 24 h after treatment, with oxalate concentrations below the detection limit of the colorimetric method. Furthermore, the decrease in oxalate production was still notable 48 h after treatment, with reductions in the extracellular oxalate concentration of 70% (**2l**), 60% (**1** and **11**) and 50% (**2b**). Compound **2l**, with a secondary propargyl amine fragment, resulted especially interesting. RO suffered a decrease of 90–100% 24 h after the treatment with **2l**, which was conserved up to 70–90% after 48 h in the three types of PHs (Table 4). Other interesting compounds, considering their activity on the three types of PHs, were **1**, **2b**, **2a** and **11**. All of them exceed the phenotypic activity of the clinically used LDHi stiripentol, in PH2 and PH3 cells (Table 4). Unfortunately, the good activity found for **9f** on recombinant enzymes did not translate into a good phenotypic effect on cells. The reason for this loss of activity could be due to difficulties in crossing the cell membrane due to the presence of two carboxylic functionalities. This agrees with the good phenotypic activity found for compound **11**, lacking the second carboxylic acid. Further studies will be followed to assess this issue.

The most active compounds in terms of RO (**2b**, **2l** and **11**) were analyzed to determine their EC_{50} in *Agxt1*$^{-/-}$ mouse hepatocytes and compared to the lead compound **1** [1] (Table 5). The branched molecule **11** presented an EC_{50} value in the three-digit nanomolar scale at 24 and 48 h. Regarding the linear amines, the substitution of the formyl group of **1** with a *p*-nitroaniline moiety (**2b**) also led to an important improvement on the EC_{50} value, both after 24 h or 48 h after treatment. Interestingly, the propargyl amine fragment of **2l**, although yielding no change on the oxalate production after 24 h of treatment with respect to **1**, it indeed produced a more lasting effect. Moreover, compound **2l** presented EC_{50} values below or close to 2 μM in PH2 and PH3 cells.

In summary, the new compounds **2b**, **2l** and **11** show promising oxalate-lowering activities in hyperoxaluric mouse hepatocytes, improving the activity already observed for compound **1** in terms of potency and duration. Experimental K_i values on enzymes are in consistence with EC_{50} values found in cells. Compound **11** was made in order to obtain information about the role of the second salicylic head in the biological activity of the tertiary amines type **9f** and **9l** and was not initially included in the anti-inflammatory and docking studies. The good phenotypic activity on hyperoxaluric cells that was found for **11** prompts us to further develop this type of monocarboxylic branched molecules as well as to optimize their synthesis in future work.

Table 4
Relative oxalate output on hyperoxaluric mouse primary hepatocytes treated with double GO/LDHA inhibitors.

Compound	PH1[a]		PH2[b]		PH3[c]	
	24h	48h	24h	48h	24h	48h
1	−0.06 ± 0.29	0.38 ± 0.24	0.13 ± 0.22	0.14 ± 0.25	0.38 ± 0.66	0.54 ± 0.10
2a	0.19 ± 0.20	0.57 ± 0.01	0.41 ± 0.02	0.56 ± 0.01	0.26 ± 0.07	0.18 ± 0.18
2b	0.04 ± 0.06	0.50 ± 0.07	0.60 ± 0.34	0.88 ± 0.03	0.18 ± 0.26	0.10 ± 0.15
2e	0.50 ± 0.25	0.79 ± 0.04	0.40 ± 0.04	0.52 ± 0.03	0.20 ± 0.05	0.14 ± 0.13
2f	0.18 ± 0.07	0.63 ± 0.12	–	–	–	–
2l	−0.08 ± 0.05	0.29 ± 0.06	0.10 ± 0.17	0.21 ± 0.36	0.13 ± 0.22	0.12 ± 0.24
9f	0.66 ± 0.22	0.76 ± 0.12	0.59 ± 0.06	0.76 ± 0.06	0.41 ± 0.07	0.47 ± 0.04
9l	0.44 ± 0.17	–	0.20 ± 0.35	0.25 ± 0.44	0.21 ± 0.36	0.52 ± 0.07
11	−0.09 ± 0.09	0.42 ± 0.05	0.31 ± 0.27	0.34 ± 0.30	0.22 ± 0.38	0.30 ± 0.19
Stiripentol	–	–	0.27 ± 0.08	0.33 ± 0.01	0.70 ± 0.04	0.49 ± 0.05

Relative oxalate (RO) is the oxalate concentration found in the extracellular medium after treatment with an inhibitor (RO ≤ 1), expressed relative to the oxalate concentration found in the extracellular medium in the absence of the inhibitor (RO = 1) (for each inhibitor, mean of three/four replicates with standard deviations are given). All the compounds were tested at a dose of 10 μM. RO negative values indicate concentrations of oxalate below the detection limit. RO was determined at 24 h and 48 h post-treatment, in.

[a] *Agxt1*$^{-/-}$ mouse hepatocytes cultured with 5 mM glycolate.

[b] *Grhpr*$^{-/-}$ mouse hepatocytes cultured with 10 mM glycolate.

[c] *Hoga1*$^{-/-}$ mouse hepatocytes cultured with 10 mM hydroxyproline.

2.5. Evaluation of the anti-inflammatory activity and the renal safety

We evaluated the capacity of our compounds to produce any anti-inflammatory effect through pro-inflammatory cytokine inhibition or COX-1/COX-2 inhibition and we also searched for any renal cytotoxicity (Table S160) (full data in Supporting *Information*, section S13). Most of the compounds exhibited no inhibitory activity after screening on recombinant COX-1 (ovine) and COX-2 (human). Compound **9f**, the most potent compound against COX-1, exerted an IC_{50} value of 24 μM against this isozyme and compounds **2a** and **2e** were the only ones inhibiting COX-2 (IC_{50} values 35 and 36 μM, respectively). In any case, IC_{50} values against COX isozymes resulted between 9-fold and 60-fold higher than the IC_{50} values on *h*GO and *h*LDHA. None of the studied compounds produced a significant decrease of TNF-α, IL-6 or IL-1β in the supernatants of cultures of human monocyte model THP-1 (ATCC® TIB-202™) treated with LPS. The renal safety of our compounds was tested *in vitro* by measuring cellular toxicity, using the MTT metabolic test, on the

Table 5
EC_{50} values of double GO/LDHA inhibitors on hyperoxaluric mouse primary hepatocytes (oxalate output).

		EC_{50} 24h (μM)	EC_{50} 48h (μM)
PH1	**1**	3.5 ± 1.2	8.4 ± 1.1
	2b	0.6 ± 0.2	1.6 ± 0.2
	2l	4.0 ± 0.9	3.8 ± 1.1
	11	0.5 ± 0.1	0.6 ± 0.04
PH2	**1**	1.8 ± 0.5	1.9 ± 0.1
	2l	1.2 ± 0.4	2.7 ± 0.2
PH3	**2l**	1.7 ± 0.2	1.9 ± 0.1

Results expressed as the mean of three/four replicates (8 concentrations of inhibitor each; 5 mM glycolate, 10 mM glycolate and 10 mM hydroxyproline for PH1, PH2 and PH3 respectively) with standard deviations.

kidney-derived lines HEK-293 (ECACC 85120602) and 786-O (ATCC CRL-1932™) and using doxorubicin as a positive control. None of the compounds showed cytotoxicity in any of the tested cells in the range of concentrations studied (results not shown).

2.6. Biological evaluation of **2l** in PH1 mice: urine oxalate determination after oral administration

Compound **2l**, showing the best phenotypic profile in hepatocyte cultures, was chosen for *in vivo* evaluation. *Agxt1*$^{-/-}$ mice were treated orally with **2l** at daily doses of 20 mg/kg body weight during 5 days. After this time, oxalate levels in urine suffered a significant 50% reduction (normalized with creatinine) compared to pre-treated mice (control) (Fig. 2A). The decrease was statistically significant after two doses (day 2). Besides, an increase in urine glycolate was observed compared to pre-treated mice (control) (Fig. 2B). The treatment was well tolerated by the mice, without clinical signs of toxicity. These results suggest that compound **2l** can effectively produce a decrease of oxalate excretion in PH1 mice and GO/LDHA inhibition is a feasible pharmacological mechanism happening *in vivo*. This drug is more potent *in vivo* (mice) than other known GOi's such as CCPST [3]. This can be considered as a proof-of-concept of the potential of salicylic derivatives as *anti*-hyperoxaluric drugs.

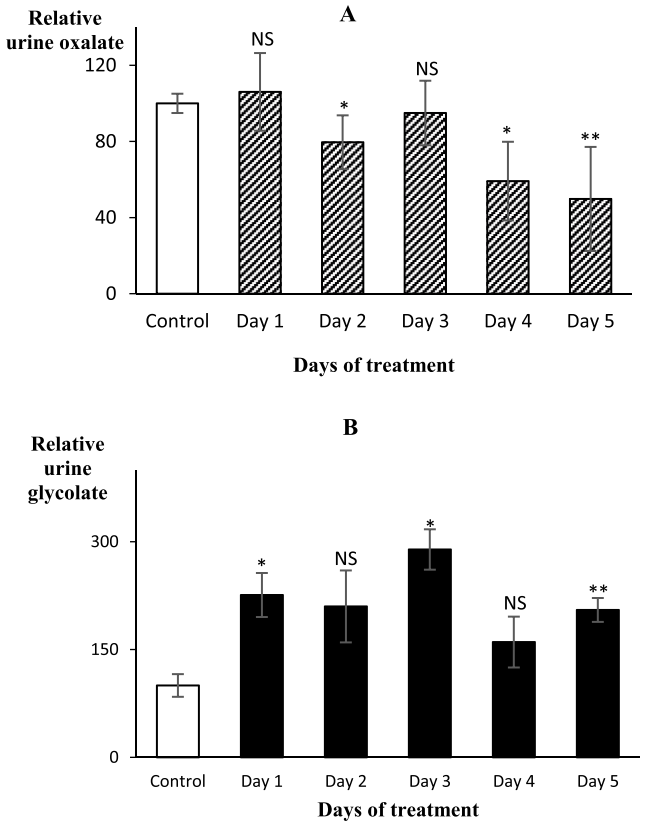

Fig. 2. *In vivo* effects of **2l** treatment in PH1 mice. Relative (%) 24-h oxalate (A) and glycolate (B) urine excretion in *Agxt1*$^{-/-}$ mice after daily administration of **2l** during 5 days. (A) Relative 24-h oxalate excretion normalized with creatinine. Significant reduction in oxalate levels compared to basal oxaluria in pre-treated *Agxt1*$^{-/-}$ mice (control). After 5 doses of **2l**, oxalate levels resulted 50% lower than before the treatment. (B) Relative 24-h glycolate excretion. Significant increase in glycolate levels compared to basal glycolate excretion in pre-treated *Agxt1*$^{-/-}$ mice (control). Values represented as mean ± SE of ten male *Agxt1*$^{-/-}$ mice. Paired *t*-test statistical analysis (*p < 0.05, **p < 0.01).

2.7. Docking results in hGO

We used three conformations of the enzyme *h*GO to carry out docking studies: the open conformation PDB ID 2RDT, the closed conformation PDB ID 2RDU and a human homology modelled intermediate open/closed conformation prepared using as template the spinach GO, PDB ID 1AL7 [51] (Supporting *Information*, section S14.1). Our docking results on *h*GO suggest the SAs present two main regions of interaction inside the enzyme: the active site/hydrophobic channel region and an alternative region located above the catalytic centre and behind the αE helix (detailed docking interactions and affinity energy tables in sections S14.2, S14.3). Interaction within the active site is the preferred binding mode for most of the studied SAs, while bonding at the alternative allosteric region occurs when the substrate occupies the active centre (closed 2RDU conformation). However, compound **2l** binds the alternative region even when the active centre is unoccupied (intermediate open/closed conformation of the homology model-1AL7). In fact, the pose of **2l** was almost identical in both enzyme models, forming the same number of H-bonds with the same residues (Fig. 3). The alternative binding region could be considered an allosteric inhibition site, supporting and giving a plausible explanation to the experimental evidence that the studied SAs are mixed type noncompetitive inhibitors with preference for the enzyme *vs* the enzyme-substrate complex (α > 1). Furthermore, compound **2l**, for which docking studies predict a more feasible binding at the allosteric site than for the rest of the salicylates [$\Delta G_{2RDT\text{-}2l}$ (-8.61) ≈ $\Delta G_{2RDU\text{-}2l}$ (-7.17)], is also the compound with the lowest experimental α value (closer to 1) determined in our experiment of inhibition kinetics on *h*GO (Table 2). The length of the side chain of the molecule appears to be critical to allow a reinforcement of the interaction at hydrophobic regions located near the active site (Figs. S75–S80). Those salicylates binding the pivotal residue Trp 110, present better inhibitory activities in the experimental inhibition assays on recombinant *h*GO.

2.8. Docking results in hLDH isozymes

Docking studies on enzyme *h*LDHA were carried out on published *h*LDHA crystal structures with PDB IDs 1I10, 4L4S and 6SBU [46,52,53]. Docking studies on enzyme *h*LDHB were carried out on the published

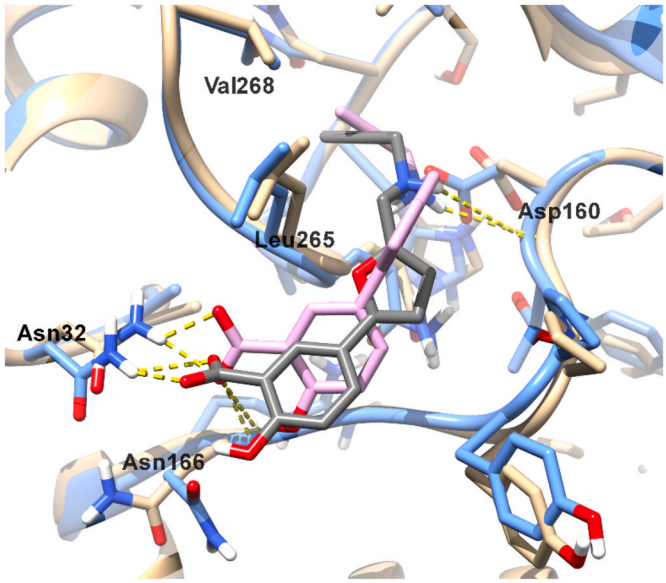

Fig. 3. Superposition of the predicted binding orientations of **2l** (light pink) in 2RDU (tan) and **2l** (grey) in *h*GO homology model (light blue). In both cases, **2l** occupies an allosteric binding site. Hydrogen bonds are represented by dashed yellow lines.

*h*LDHB crystal structure with PDB ID 1I0Z [53]. Detailed docking interactions and binding affinity tables are included as Supporting *Information* (sections S15-S17). Known LDHi's can bind the substrate binding pocket [54–58] as pyruvate-competing analogues, or the cofactor binding site, competing with NADH [57–59]. Besides, recent investigations have found an allosteric binding site for selective *h*LDHA inhibition (L5N binding site) located at the interface between two LDHA monomers (chains A and B) [46]. It is also known that LDH presents a catalytic mechanism with rate-promoting vibration (RPV) [60] and, for *h*LDHB, a RPV region has been defined all along the donor/acceptor axis stretching beyond the active site [61,62]. A potential RPV-allosteric binding site for *h*LDHB inhibition has been suggested to be located in a small area close to the RPV residues [47]. Several molecules with complementary structure to the RPV-allosteric site have been docked in this region, being 2-chloro-*N*-(3,5-dihydroxyphenyl)acetamide (CPA) the top scorer compound [47].

2.8.1. Docking in the catalytic groove of hLDH isozymes

Our results suggest that SAs are not substrate-binding-pocket specific. In fact, the aminomethylfuryl SAs prefer binding at the catalytic site entrance channel, region where the phosphate groups of NADH bind. The molecules situate their salicylic end at the active site entrance and stretch towards the hydrophobic cleft (both of which are sites of cofactor binding). Interactions are identical in both isozymes. There are key residues with which most of the studied salicylates interact. All of these residues participate in the NADH binding at the entrance to the active channel or at the hydrophobic cleft.

2.8.2. Docking in the allosteric site of the inhibitor L5N in hLDHA

We found that our compounds can use their salicylic head along with their side chain and, in most cases, also the secondary or tertiary amine group to establish binding interactions in the allosteric binding site of L5N. In all cases, the salicylic head is oriented towards the subunit B of the *h*LDHA while the side chain can interact with both A and/or B subunits. It is worth highlighting that ligands **2e**, **9f** and **9l**, present comparable binding energies to that of the redocked cognate ligand L5N (Table S169). It also stands out that, for most of the salicylates, binding at the allosteric site is equivalent in terms of binding energy, to binding at the cofactor region of the apoproteins (Table S168).

2.8.3. Docking in the RPV-allosteric site of hLDH isozymes

All linear compounds were able to bind the RPV allosteric site and establish the same interactions that CPA, with residues Tyr247 and Gln30, in the two subunits, A and B, which compose this allosteric site (Fig. S90). Other important interactions of linear salicylates inside this RPV-allosteric site are the ones with Trp250-A and Tyr27-B. Besides, the linear compounds bind to Lys57, at the active site entrance of both subunits. To our knowledge, the RPV region has not been confirmed as an allosteric inhibition site in *h*LDHA. We found a small but significant difference in this area when comparing the residues of the two isozymes: Ala29 and Ser248 in *h*LDHA correspond to Gln30 and Asn249 in *h*LDHB. The more voluminous Gln30 and Asn249 in *h*LDHB create a smaller area which limits the size and number of possible inhibitors fitting into the allosteric site; on the contrary, Ala29 and Gln30 in *h*LDHA allows for bigger ligands to fit in. These differences point to a potential allosteric binding site that could allow the design of selective ligands (full details in section S17.2). We docked CPA on this region of *h*LDHA and compared the results with those of *h*LDHB (Table S172, Fig. S91). While the binding poses are similar in both isozymes, up to three H-bonds interactions are missing on *h*LDHA when compared with the binding pose on *h*LDHB. These missing H-bonds are established with the residues that are not present in *h*LDHA but they are in *h*LDHB: Gln30-B (one H-bond) and Asn249-A (two H-bonds). We must also highlight that the bulky molecules **9f** and **9l** did not fit in the RPV-site in *h*LDHB but they did fit and indeed obtained the best docking scores on the very same region of *h*LDHA. This agrees with the experimental evidence that compound **9f** presents a favourable selectivity for *h*LDHA *vs* *h*LDHB in terms of K_i values comparison. The binding affinities found for our salicylates in this RPV-allosteric site of *h*LDHB and *h*LDHA resulted comparable to the ones of the redocked CPA or even slightly better (Table S172).

3. Conclusion

We have proved that salicylic derivatives are dual inhibitors of the enzymes *h*GO and *h*LDHA [1]. We have prepared and evaluated a new family of 5-(5-aminomethyl)furyl SAs analogues of the parent compound **1**. These new molecules present improved inhibitory activity against *h*GO and *h*LDHA as well as better phenotypic activity *in vitro*. The novel compounds are made from **1** in a single step synthesis. These compounds behave as reversible noncompetitive inhibitors (*vs* substrate) of both enzymes and are active against the three types of PHs (mouse PH models, *in vitro* cell assays). Further research will determine if there is a synergistic effect of the double target mechanism. Compounds **2l** and **11** present the most promising biological profiles. Their lasting phenotypic activity is extended to the three types of PHs. Compound **2l** is a stable molecule synthesized with an overall yield of 76% in two steps. Besides, compound **2l** is active after oral administration to *Agxt1*$^{-/-}$ mice. Branched molecules type **11** could afford selective *h*LDHA isozyme inhibitors, but they need further development in terms of synthesis and bioavailability optimization. Docking on *h*GO suggests that the SAs studied are capable of binding the substrate site, but also an alternative region located next to the catalytic centre. There are no former evidences in literature of GOi's binding at this alternative region. In the case of *h*LDH, docking studies suggest that our SAs preferably bind the cofactor site. In addition, these molecules can also fit previously described allosteric binding sites in *h*LDHA (L5N binding site and CPA binding site) and *h*LDHB (CPA binding site). The narrower structure of the CPA binding site in *h*LDHB *vs* the same region of *h*LDHA, prevents the binding of bulky molecules to the first isozyme and gives the chance for the design of selective hits against *h*LDHA *vs* *h*LDHB. This is an important observation given the structural similarity of these two isozymes.

4. Experimental section

4.1. General experimental methods

All solvents and chemicals were used as purchased without further purification. The progress of the reactions was controlled by thin layer chromatography (TLC) on aluminium plates (Merck AL Silicagel 60 F254) and detected by UV lamp (254 nm) or employing a solution of vanillin (6 g) and concentrated sulfuric acid (2.5 mL) in ethanol (250 mL) and heating. Purification by flash chromatography was performed on Silicagel Merck 60 (230–400 mesh ASTM). The non-crystalline compounds were shown to be homogeneous by chromatographic methods and characterized by NMR and HRMS. ^{1}H NMR and ^{13}C NMR spectra have been recorded in a 2-channel 300 MHz Varian Inova Unity, a 2-channel 400 MHz and a 4-channel 600 MHz Varian Direct Drive spectrometers using DMSO-d_6 or CD_3OD. Chemical shifts (δ) are quoted in parts per million (ppm) and are referenced to residual H in the deuterated solvent as the internal standard. Coupling constants (J) are expressed in Hz. Splitting patterns are designated as follows: s, singlet; d, doublet; dd, double doublet; m, multiplet; q, quadruplet; t, triplet; p, pentet. High resolution mass spectra (HRMS) were recorded by time of flight (TOF) mass spectrometry with electrospray ionization (ESI) in positive or negative mode, using a time of flight apparatus with orthogonal acceleration LCT Premier™. Purity of the compounds was assessed by HPLC using an Agilent 1200 instrument with diode-array detector equipped with a Zorbax Eclipse XDB-C18 4.6 × 150 mm column. Column temperature was set at 25 °C. Absorbance was measured at 214 and 254 nm. Purity of most final compounds was higher than 95%

and in every case higher than 90%. Melting points (mp) were taken in open capillaries on a Gallenkamp Melting Point Apparatus and are uncorrected. For colorimetric interference test, absorbance was measured at 515 and 590 nm. Recombinant enzymes *m*GO and *h*GO were obtained from BL21 (DE3) *Escherichia coli* transformed with recombinant pET-15 b expression vectors carrying the coding sequence of mouse or human *Hao1* cDNA, respectively, purified and stored in absence of glycerol. *h*LDHA and *h*LDHB (Novusbio) as well as COX-1 and COX-2 (BioVision) enzymes were obtained from commercial sources. A Multiskan™ FC Microplate Photometer (Thermo Fisher) was used to measure absorbance and an EnSpire® Multimode Plate Reader (PerkinElmer) was used to measure fluorescence. For fluorometric assays, OptiPlate black opaque 96-well microplates (PerkinElmer) were used. For all assays, the final volume in each well was 200 μL. Multi-channel pipettes were used for the addition of the reagents in the wells. For the most potent GO inhibitors, fluorescence interference tests were performed by measuring fluorescence with λ_{ex} 560 nm and λ_{em} 590 nm. Interferences in the kinetic fluorometric protocol were discarded as the slope in the linear interval was corrected by subtraction of the baseline reading registered before the addition of the substrate. All graphic and statistical analyses were conducted using GraphPad Prism v.6 (GraphPad Software Inc., San Diego, CA) and Microsoft Excel 2013 (Microsoft Office Professional Plus 2013).

HPLC methods for purity determination:

General HPLC set up: Detector $\lambda = 214$, 254 nm; Flow 0.8 mL/min, solvent A [water (0.1% HCOOH)/ACN (0.1% HCOOH)]; solvent B [ACN (0.1% HCOOH) 100%]:

HPLC set up for compounds **2h**, **2j**, **2k**, **2l**: Solvent A (90/10). Isocratic A 2 min + gradient A→ B 17 min + isocratic B 2 min (Method 1).

HPLC set up for compounds **1**, **2b**, **2e**, **2f**, **2g**, **2i**, **9f**, **9l**, **11**: Solvent A (80/20). Isocratic A 2 min + gradient A→B 17 min + isocratic B 2 min (Method 2).

HPLC set up for compound **2a**: Solvent A (70/30). Isocratic A 2 min + gradient A→B 17 min + isocratic B 2 min (Method 3).

4.2. Chemical methods

4.2.1. 5-(5-Formylfuran-2-yl)-2-hydroxybenzoic acid (1)

A solution of potassium carbonate (90 mg, 0.648 mmol, 3 equiv) in water (1 mL) was prepared in a glass tube equipped with a stirring bar. After dissolution, ethanol was added (1 mL) and the mixture was degassed by bubbling with argon. Consecutively, methyl 2-hydroxy-5-iodobenzoate (60 mg, 0.216 mmol, 1 equiv), 5-formylfuran-2-boronic acid (45 mg, 0.324 mmol, 1.5 equiv), and PdEnCat® 30 (33 mg, 0.113 mmol; 0.4 mmol/g Pd, 6 mol%) were added in that sequence. The mixture was then degassed by argon bubbling during 10 min, after which the tube was sealed. The reaction was heated at 80 °C during 24 h. After this time, the reaction crude was filtered (washing with methanol) and the filtrate was evaporated in rotavapor. The residue was dissolved in water, cooled to 0 °C, and acidified with HCl 10%. After evaporation under vacuum, the final crude was purified by flash column chromatography on silica gel (gradient elution DCM:MeOH 20:1 → 8:2) and compound **1** was obtained as a brown solid (mp 232 °C) in quantitative yield (50 mg, 0.215 mmol). ^{1}H NMR (400 MHz, DMSO-d_6) δ 9.51 (s, 1H), 8.21 (d, $J = 2.4$ Hz, 1H), 7.70 (dd, $J = 8.5$, 2.5 Hz, 1H), 7.60 (d, $J = 3.8$ Hz, 1H), 7.00 (d, $J = 3.8$ Hz, 1H), 6.76 (d, $J = 8.6$ Hz, 1H).^{13}C NMR (101 MHz, DMSO-d_6) δ 176.7 (CHO), 170.8 (CO), 165.5 (C), 159.8 (C), 150.8 (C), 129.2 (CH), 127.1 (CH), 120.0 (C), 117.3 (CH), 116.64, 116.62 (C, CH), 105.9 (CH). HRMS (TOF, ES$^-$): *m/z* calcd. For $C_{12}H_7O_5$ (M-H$^+$)$^-$ 231.0300, found 231.0293. HPLC: ($\lambda = 254$ nm): 100%; $t_R = 11.02$ min (HPLC method 2).

4.2.2. N-[4-(4-Aminobenzoyl)phenyl]hex-5-ynamide (3e)

[63]. In a round bottom flask equipped with a stirring bar and under argon atmosphere, 156 μL of 5-hexynoic acid (1.413 mmol), 191 mg of HOBt (1.403 mmol) and 271 mg of EDC·HCl (1.413 mmol) were dissolved in 1 mL of anhydrous DMF and stirred at rt for 10 min. Then, in a different flask, 150 mg of 4,4′-diaminobenzophenone (0.706 mmol) were dissolved in 2.6 mL of anhydrous DMF and the first mixture was added over this one in portions along 1 h. The reaction was allowed to stir for 24 h at rt. After that time, 100 mL of EtOAc were added and the organic layer was washed with a saturated aqueous solution of $NaHCO_3$ (2 x 100 mL), with a 10% citric acid solution (2 x100 mL) and finally with HCl 3 N (150 mL) to remove the 4,4′-diaminobenzophenone. The organic layer was collected and neutralized at 0 °C with NaOH 20% in order to precipitate the final product, which was extracted with EtOAc, dried over Na_2SO_4, filtered and concentred in rotavapor. Yellow solid (mp 179–181 °C), 32% yield (71 mg, 0.232 mmol). ^{1}H NMR (400 MHz, CD_3OD) δ 7.79–7.67 (m, 4H), 7.64 (d, $J = 8.7$ Hz, 2H), 6.72 (d, $J = 8.6$ Hz, 2H), 2.59 (t, $J = 7.4$ Hz, 2H), 2.41–2.25 (m, 3H), 1.94 (p, $J = 7.0$ Hz, 2H). ^{13}C NMR (101 MHz, CD_3OD) δ 196.6 (CO), 174.0 (CO), 155.1 (C), 143.3 (C), 135.3 (C), 134.0 (2CH), 131.7 (2CH), 126.4 (C), 120.0 (2CH), 114.1 (2CH), 84.1 (C), 70.3 (CH), 36.6 (CH2), 25.5 (CH2), 18.6 (CH2). HRMS (TOF, ES$^+$): *m/z* calcd. For $C_{19}H_{19}N_2O_2$ (M + H$^+$)$^+$ 307.1447, found 307.1434 (deviation −4.2 ppm). HPLC: ($\lambda = 254$ nm): 100%; $t_R = 12.65$ min ($\lambda = 214$ nm): 100%; $t_R = 12.65$ min (HPLC method 2).

4.2.3. General procedure for reductive amination

In a dry flask, under argon, a solution of **1** (1 equiv) and the corresponding amine (**3**) (1.2 equiv) was made in anhydrous MeOH. Afterwards, anhydrous DCM, and activated 3 Å molecular sieves were added. The mixture was then stirred at rt, in darkness conditions, until formation of the intermediate imine (TLC). Afterwards, the reaction was cooled to 0 °C for the addition of sodium triacetoxyborohydride (2.5 equiv). The reaction was left to stir at rt until the disappearance of the imine (TLC) and was then quenched by addition of H_2O after cooling at 0 °C. Molecular sieves were removed by filtration and the filtrate was concentrated in rotavapor keeping temperature under 30 °C. The residue was purified by flash chromatography. For unstable amines acid silica was neutralized before loading the crude by using mobile phases containing methanolic ammonia (7 N) or NH_4OH (32%)/MeOH 2/100.

4.2.3.1. Ammonium 5-{5-[N-(p-bromophenyl)aminomethyl]-2-furyl}-2-hydroxybenzoate (2a). Reductive amination general procedure, **1** (100 mg, 0.431 mmol), *p*-bromoaniline (**3a**) (89 mg, 0.517 mmol), sodium triacetoxyborohydride (183 mg, 0.862 mmol), DCM (6 mL), MeOH (2 mL). Imine formation, 1 h; reduction, 2 h. Purification: Gradient elution using DCM/[NH_4OH (32%)/MeOH 2/100] 10:0.1 → 10:0.6. Yield: 45% (80 mg, 0.197 mmol) (orange solid, mp 115–117 °C decomposition). ^{1}H NMR (400 MHz, CD_3OD) δ 8.17 (d, $J = 1.9$ Hz, 1H), 7.60 (dd, $J = 8.5$, 2.0 Hz, 1H), 7.20 (d, $J = 8.7$ Hz, 2H), 6.83 (d, $J = 8.5$ Hz, 1H), 6.64 (d, $J = 8.7$ Hz, 2H), 6.48 (d, $J = 3.1$ Hz, 1H), 6.27 (d, $J = 3.0$ Hz, 1H), 4.30 (s, 2H). ^{13}C NMR (101 MHz, CD_3OD) δ 175.4 (CO), 162.1 (C), 154.6 (C), 153.0 (C), 148.9 (C), 132.6 (2CH), 129.6 (CH), 126.9 (CH), 123.1 (C), 119.2 (C), 117.7 (CH), 115.8 (2CH), 109.9 (CH), 109.4 (C), 104.6 (CH), 41.9 (CH2). HRMS (TOF, ES$^-$): *m/z* calcd. For $C_{18}H_{13}NO_4Br$ (M-H$^+$)$^-$ 386.0028, found 386.0051 (deviation +6.0 ppm). HPLC: ($\lambda = 254$ nm): 99%; $t_R = 16.41$ min ($\lambda = 214$ nm): 97%; $t_R = 16.79$ min (unstable under HPLC conditions) (HPLC method 3).

4.2.3.2. Ammonium 2-hydroxy-5-{5-[N-(p-nitrophenyl)aminomethyl]-2-furyl}benzoate (2b). Reductive amination general procedure, **1** (100 mg, 0.431 mmol), *p*-nitroaniline (**3b**) (77 mg, 0.560 mmol), sodium triacetoxyborohydride (183 mg, 0.862 mmol), DCM/MeOH 3/1 (4 mL). Imine formation, 5 h; reduction, 3 h. Purification: Elution using DCM/[NH_4OH (32%)/MeOH 2/100] 10:0.1. Yield: 24% (39 mg, 0.105 mmol) (yellow solid, mp 159–161 °C). ^{1}H NMR (400 MHz, CD_3OD) δ 8.20 (d, $J = 2.0$ Hz, 1H), 8.07 (d, $J = 9.2$ Hz, 2H), 7.62 (dd, $J = 8.4$, 1.6 Hz, 1H), 6.85 (d, $J = 8.5$ Hz, 1H), 6.76 (d, $J = 9.1$ Hz, 2H), 6.52 (d, $J = 3.2$ Hz, 1H), 6.36 (d, $J = 3.2$ Hz, 1H), 4.47 (s, 2H). ^{13}C NMR (101 MHz, CD_3OD) δ 175.6 (CO), 162.2 (C), 155.5 (C), 155.2 (C), 151.6 (C), 138.5 (C), 129.4

(CH), 127.1 (CH), 127.0 (CH), 122.8 (C), 119.8 (C), 117.6 (CH), 112.2 (CH), 110.4 (CH), 104.5 (CH), 41.0 (CH2). HRMS (TOF, ES^-): *m/z* calcd. For $C_{18}H_{13}N_2O_6$ $(M\text{-}H^+)^-$ 353.0774, found 353.0778 (deviation +1.1 ppm). HPLC: ($\lambda = 254$ nm): 100%; $t_R = 15.87$ min ($\lambda = 214$ nm): 100%; $t_R = 15.87$ min (HPLC method 2).

*4.2.3.3. Ammonium 5-{5-{{N-{4-[4-(hex-5-ynamido)benzoyl]phenyl} amino}methyl}furan-2-yl}-2-hydroxybenzoate (**2e**).* Reductive amination general procedure, **1** (31 mg, 0.133 mmol), **3e** (53 mg, 0.172 mmol), sodium triacetoxyborohydride (56 mg, 0.266 mmol), DCM/MeOH 3/1 (4 mL). Imine formation, 2 h; reduction, 2 h. Purification: Elution AcOEt/ACN/MeOH–NH_3 (7 N) 70:5:2.5 → 70:10:5. Yield: 69% (50 mg, 0.092 mmol) (orange solid, mp 148–150 °C). ^{1}H NMR (400 MHz, CD_3OD) δ 8.20 (d, $J = 2.3$ Hz, 1H), 7.79–7.65 (m, 7H), 6.90 (d, $J = 8.6$ Hz, 1H), 6.80 (d, $J = 8.8$ Hz, 2H), 6.56 (d, $J = 3.3$ Hz, 1H), 6.37 (d, $J = 3.3$ Hz, 1H), 4.48 (s, 2H), 2.58 (t, $J = 7.4$ Hz, 2H), 2.36–2.27 (m, 3H), 1.93 (m, $J = 7.0$ Hz, 2H). ^{13}C NMR (101 MHz, CD_3OD) δ 196.6 (CO), 174.8 (CO), 174.0 (CO), 162.2 (C), 154.5 (C), 154.3 (C), 152.6 (C), 143.3 (C), 135.3 (C), 133.9 (CH), 131.7 (CH), 130.4 (CH), 126.7 (CH), 126.4 (C), 123.3 (C), 120.0 (CH), 118.0 (CH), 117.5 (C), 112.5 (CH), 110.2 (CH), 105.0 (CH), 84.1 (C), 70.3 (CH), 41.0 (CH2), 36.6 (CH2), 25.5 (CH2), 18.6 (CH2). HRMS (TOF, ES^-): *m/z* calcd. For $C_{31}H_{25}N_2O_6$ $(M\text{-}H^+)^-$ 521.1713, found 521.1703 (deviation −1.9 ppm). HPLC: ($\lambda = 254$ nm): 84%; $t_R = 16.12$ min ($\lambda = 214$ nm): 76%; $t_R = 16.12$ min (HPLC method 2).

4.2.3.4. Ammonium 5-[5-(benzylaminomethyl)-2-furyl]-2-hydroxybenzoate (2f). Reductive amination general procedure, **1** (92 mg, 0.397 mmol), benzyl amine (**3f**) (56.3 μL, 0.516 mmol), sodium triacetoxyborohydride (168 mg, 0.794 mmol), DCM (3 mL), MeOH (1 mL). Imine formation, 24 h; reduction, 2 h. Purification: Gradient elution using AcOEt/ACN/MeOH–NH_3 (7 N)/H_2O 70:2.5:1.25:1.25 → 7:5:2.5:2.5. Yield: 67% (91 mg, 0.267 mmol) (yellow solid, mp 182–185 °C). ^{1}H NMR (400 MHz, DMSO-d_6) δ 8.11 (s, 1H), 7.68–7.27 (m, 6H), 6.81–6.50 (m, 3H), 4.21 (s, 2H), 4.16 (s, 2H). ^{13}C NMR (101 MHz, DMSO-d_6) δ 171.3 (CO), 163.2 (C), 154.9 (C), 144.7 (C), 132.7 (C), 129.8 (2CH), 128.66 (CH), 128.60 (2CH), 127.7 (CH), 125.6 (CH), 119.8 (C), 118.6 (C), 116.5 (CH), 113.6 (CH), 103.4 (CH), 49.7 (CH2), 42.5 (CH2). HRMS (TOF, ES^-): *m/z* calcd. For $C_{19}H_{16}NO_4$ $(M\text{-}H^+)^-$ 322.1079, found 322.1087 (deviation +2.5 ppm). HPLC: ($\lambda = 254$ nm): 98%; $t_R = 8.98$ min ($\lambda = 214$ nm): 98%; $t_R = 8.98$ min (HPLC method 2).

4.2.3.5. Ammonium 2-hydroxy-5-{5-[N-(p-nitrobenzyl)aminomethyl]-2-furyl}benzoate (2g). Reductive amination general procedure, **1** (100 mg, 0.431 mmol), 4-nitrobenzylamine hydrochloride (**3g**) (105.60 mg, 0.559 mmol), sodium triacetoxyborohydride (183 mg, 0.861 mmol), DCM (3 mL), MeOH (1 mL). Imine formation, 24 h; reduction, 3 h. Purification: Gradient elution using AcOEt/ACN/MeOH–NH_3 (7 N)/H_2O 70:2.5:1.25:1.25 → 70:10:5:5. Yield: 48% (80 mg, 0.208 mmol) (yellow solid, mp 172–175 °C). ^{1}H NMR (400 MHz, DMSO-d_6) δ 8.27 (d, $J = 8.7$ Hz, 2H), 8.08 (d, $J = 2.4$ Hz, 1H), 7.75 (d, $J = 8.7$ Hz, 2H), 7.56 (dd, $J = 8.5$, 2.5 Hz, 1H), 6.72 (d, $J = 8.5$ Hz, 1H), 6.65 (d, $J = 3.3$ Hz, 1H), 6.56 (d, $J = 3.3$ Hz, 1H), 4.25 (s, 2H), 4.18 (s, 2H). ^{13}C NMR (101 MHz, DMSO-d_6) δ 170.9 (CO), 163.2 (C), 154.7 (C), 151.1 (C), 147.3 (C), 130.7 (2CH), 127.9 (CH), 125.4 (CH), 123.5 (2CH), 119.2 (C), 118.7 (C), 116.7 (CH), 116.6 (C), 113.0 (CH), 103.4 (CH), 49.3 (CH2), 43.3 (CH2). HRMS (TOF, ES^-): *m/z* calcd. For $C_{19}H_{15}N_2O_6$ $(M\text{-}H^+)^-$ 367.0930, found 367.0927 (deviation −0.8 ppm). HPLC: ($\lambda = 254$ nm): 96%; $t_R = 8.94$ min (HPLC method 2).

4.2.3.6. Ammonium 2-hydroxy-5-{5-[N-(p-hydroxybenzyl)aminomethyl]-2-furyl}benzoate (2h). Reductive amination general procedure, **1** (100 mg, 0.431 mmol), 4-hydroxybenzylamine (**3h**) (69 mg, 0.559 mmol), sodium triacetoxyborohydride (183 mg, 0.861 mmol), DCM (3 mL), MeOH (1 mL). Imine formation, 24 h; reduction, 3 h. Purification: Gradient elution using AcOEt/ACN/MeOH–NH_3 (7 N)/H_2O 70:2.5:1.25:1.25 → 70:10:5:5. Yield: 52% (80 mg, 0.224 mmol) (yellowish solid, mp 190 °C decomposition). ^{1}H NMR (400 MHz, DMSO-d_6) δ 9.73 (s, 1H), 8.11 (d, $J = 2.4$ Hz, 1H), 7.55 (dd, $J = 8.5$, 2.3 Hz, 1H), 7.31 (d, $J = 8.4$ Hz, 2H), 6.80 (d, $J = 8.4$ Hz, 2H), 6.70 (d, $J = 8.5$ Hz, 1H), 6.66–6.60 (m, 2H), 4.21 (s, 2H), 4.07 (s, 2H). ^{13}C NMR (101 MHz, DMSO-d_6) δ 171.1 (CO), 163.3 (C), 158.0 (C), 155.1 (C), 144.0 (C), 131.5 (2CH), 127.7 (CH), 125.6 (CH), 121.9 (C), 119.8 (C), 118.4 (C), 116.6 (CH), 115.3 (2CH), 113.9 (CH), 103.3 (CH), 49.3 (CH2), 42.1 (CH2). HRMS (TOF, ES^+): *m/z* calcd. For $C_{19}H_{18}NO_5$ $(M + H^+)^+$ 340.1185, found 340.1198 (deviation +3.8 ppm). HPLC: ($\lambda = 254$ nm): 100%; $t_R = 10.58$ min ($\lambda = 214$ nm): 99%; $t_R = 10.58$ min (HPLC method 1).

4.2.3.7. Ammonium 2-hydroxy-5-{5-[N-(p-methoxybenzyl)aminomethyl]-2-furyl}benzoate (2i). Reductive amination general procedure, **1** (100 mg, 0.431 mmol), 4-methoxybenzylamine (**3i**) (73.1 μL, 0.559 mmol), sodium triacetoxyborohydride (183 mg, 0.861 mmol), DCM (3 mL), MeOH (1 mL). Imine formation, 24 h; reduction, 3 h. Purification: Gradient elution using AcOEt/ACN/MeOH–NH_3 (7 N)/H_2O 70:2.5:1.25:1.25 → 70:10:5:5. Yield: 51% (82 mg, 0.221 mmol) (yellowish solid, mp 200–203 °C). ^{1}H NMR (600 MHz, DMSO-d_6) δ 9.31 (s, 1H), 8.10 (d, $J = 2.5$ Hz, 1H), 7.53 (dd, $J = 8.4$, 2.0 Hz, 1H), 7.42 (d, $J = 8.6$ Hz, 2H), 6.99 (d, $J = 8.7$ Hz, 2H), 6.68 (d, $J = 8.5$ Hz, 1H), 6.64 (d, $J = 3.3$ Hz, 1H), 6.59 (d, $J = 3.3$ Hz, 1H), 4.19 (s, 2H), 4.11 (s, 2H), 3.76 (s, 3H). ^{13}C NMR (151 MHz, DMSO-d_6) δ 171.0 (CO), 163.5 (C), 159.6 (C), 155.1 (C), 144.3 (C), 131.4 (2CH), 127.5 (CH), 125.6 (CH), 124.2 (C), 120.1 (C), 118.2 (C), 116.5 (CH), 114.0 (2CH), 113.7 (CH), 103.2 (CH), 55.1 (CH3), 49.2 (CH2), 42.3 (CH2). HRMS (TOF, ES^+): *m/z* calcd. For $C_{20}H_{20}NO_5$ $(M + H^+)^+$ 354.1341, found 354.1335 (deviation −1.7 ppm). HPLC: ($\lambda = 254$ nm): 97%; $t_R = 9.09$ min ($\lambda = 214$ nm): 97%; $t_R = 9.09$ min (HPLC method 2).

4.2.3.8. 2-Hydroxy-5-{5-[N-(3-pyridylmethyl)aminomethyl]-2-furyl}benzoic acid (2j). Reductive amination general procedure, **1** (70 mg, 0.302 mmol), pyridin-3-ylmethanamine (**3j**) (40 μL, 0.392 mmol), sodium triacetoxyborohydride (128 mg, 0.604 mmol), DCM (3 mL), MeOH (1 mL). Imine formation, 24 h; reduction, 4 h. Purification: Gradient elution using AcOEt/ACN/MeOH/H_2O 70:5:2.5:2.5 → 6:1:1:1. Yield: 41% (40 mg, 0.123 mmol) (pale solid, mp > 300 °C). ^{1}H NMR (400 MHz, DMSO-d_6) δ 8.67 (s, 1H), 8.53 (d, $J = 3.8$ Hz, 1H), 8.05 (d, $J = 2.2$ Hz, 1H), 7.97 (d, $J = 7.7$ Hz, 1H), 7.54 (dd, $J = 8.5$, 2.5 Hz, 1H), 7.41 (dd, $J = 7.8$, 4.8 Hz, 1H), 6.69 (d, $J = 8.5$ Hz, 1H), 6.61 (d, $J = 3.2$ Hz, 1H), 6.56 (d, $J = 2.7$ Hz, 1H), 4.08 (d, $J = 3.6$ Hz, 4H). ^{13}C NMR (101 MHz, DMSO-d_6) δ 171.9 (CO), 171.3 (C), 171.3 (C), 163.0 (C), 154.4 (C), 150.6 (CH), 149.2 (CH), 137.3 (CH), 127.4 (CH), 125.5 (CH), 123.4 (CH), 120.0 (C), 118.7 (C), 116.4 (CH), 112.7 (CH), 103.3 (CH), 47.6 (CH2), 43.1 (CH2). HRMS (TOF, ES^-): *m/z* calcd. For $C_{18}H_{15}N_2O_4$ $(M\text{-}H^+)^-$ 323.1032, found 323.1056 (deviation +7.4 ppm). HPLC: ($\lambda = 254$ nm): 100%; $t_R = 8.57$ min ($\lambda = 214$ nm): 96%; $t_R = 8.57$ min (HPLC method 1).

4.2.3.9. 2-Hydroxy-5-[5-(piperidin-1-ylmethyl)-2-furyl]benzoic acid (2k). Reductive amination general procedure, **1** (100 mg, 0.431 mmol), piperidine (**3k**) (55.3 μL, 0.560 mmol), sodium triacetoxyborohydride (274 mg, 1.293 mmol), DCM (3 mL), MeOH (1 mL). Imine formation, 4 h; reduction, 4 h. Purification: Gradient elution using AcOEt/ACN/MeOH/H_2O 70:10:5:5 → 7:1:1:1. Yield: 59% (77 mg, 0.256 mmol) (brownish solid, mp 209 °C). ^{1}H NMR (400 MHz, CD_3OD) δ 8.21 (d, $J = 2.3$ Hz, 1H), 7.63 (dd, $J = 8.5$, 2.3 Hz, 1H), 6.83 (d, $J = 8.5$ Hz, 1H), 6.69–6.56 (m, 2H), 4.20 (s, 2H), 3.09 (s, 4H), 1.81 (p, $J = 5.8$ Hz, 4H), 1.62 (q, $J = 5.7$ Hz, 2H). ^{13}C NMR (101 MHz, CD_3OD) δ 175.5 (CO), 162.9 (C), 157.5 (C), 144.8 (C), 129.6 (CH), 127.5 (CH), 121.9 (C), 120.4 (C), 117.8 (CH), 116.5 (CH), 104.9 (CH), 54.2 (CH2), 54.0 (2CH2), 24.7 (2CH2), 23.1 (CH2). HRMS (TOF, ES^-): *m/z* calcd. For

$C_{17}H_{18}NO_4$ (M-H^+)$^-$ 300.1236, found 300.1264 (deviation +9.3 ppm). HPLC: (λ = 254 nm): 100%; t_R = 10.01 min (λ = 214 nm): 98%; t_R = 10.01 min (HPLC method 1).

4.2.3.10. Ammonium 2-hydroxy-5-[5-(propargylaminomethyl)-2-furyl] benzoate (2l). Reductive amination general procedure, **1** (105 mg, 0.453 mmol), propargylamine (**3l**) (38 μL, 0.588 mmol), sodium triacetoxyborohydride (192 mg, 0.904 mmol), DCM (3 mL), MeOH (1 mL). Imine formation, 24 h; reduction, 3 h. Purification: Gradient elution using AcOEt/ACN/MeOH–NH3 (7 N)/H_2O 70:2.5:1.25:1.25 → 70:10:5:5. Yield: 76% (100 mg, 0.347 mmol) (brown solid, mp 180 °C decomposition). ^{1}H NMR (300 MHz, CD_3OD) δ 8.20 (d, J = 2.3 Hz, 1H), 7.64 (dd, J = 8.6, 2.4 Hz, 1H), 6.84 (d, J = 8.7 Hz, 1H), 6.59 (s, 2H), 4.26 (s, 2H), 3.83 (d, J = 2.5 Hz, 2H), 3.11 (t, J = 2.6 Hz, 1H). ^{13}C NMR (101 MHz, CD_3OD) δ 175.4 (CO), 162.9 (C), 157.2 (C), 145.7 (C), 129.8 (CH), 127.4 (CH), 122.0 (C), 119.8 (C), 117.8 (CH), 115.1 (CH), 104.9 (CH), 78.3 (C), 75.8 (CH), 43.8 (CH2), 36.7 (CH2). HRMS (TOF, ES$^-$): *m/z* calcd. For $C_{15}H_{12}NO_4$ (M-H^+)$^-$ 270.0766, found 270.0757 (deviation −3.3 ppm). HPLC: (λ = 254 nm): 100%; t_R = 9.66 min (λ = 214 nm): 99%; t_R = 9.66 min (HPLC method 1).

4.2.3.11. 5-{5-[5-(3-Carboxy-4-hydroxyphenyl)furan-2-ylmethyl]furan-2-yl}-2-hydroxybenzoic acid (4). [36,38,39]. Formed during the chromatographic purification of secondary amines type **2**, isolated during the preparation of **2a**. Solid, mp 65 °C (decomposition). ^{1}H NMR (600 MHz, CD_3OD) δ 8.30 (s, 2H), 7.59 (dd, J = 8.6, 2.2 Hz, 2H), 6.83 (d, J = 8.5 Hz, 2H), 6.48 (d, J = 3.2 Hz, 2H), 6.20 (d, J = 3.2 Hz, 2H), 4.06 (s, 2H). ^{13}C NMR (151 MHz, CD_3OD) δ 176.4 (2CO), 161.9 (2C), 154.6 (2C), 152.1 (2C), 152.08 (2C) 129.8 (2CH), 126.9 (2CH), 123.2 (2C), 117.7 (2CH), 109.2 (2CH), 104.8 (2CH), 28.2 (CH2). HRMS (TOF, ES$^-$): *m/z* calcd. For $C_{23}H_{15}O_8$ (M-H^+)$^-$ 419.0767, found 419.0781 (deviation +3.3 ppm). HPLC: Unstable under HPLC conditions.

4.2.3.12. Ammonium 5-{5-{N-benzyl-N-[5-(3-carboxy-4-hydroxyphenyl)-2-furanylmethyl]aminomethyl}-2-furanyl}-2-hydroxybenzoate (9f). Formed during the chromatographic purification of **2f**. Brownish solid, mp 170–172 °C. ^{1}H NMR (300 MHz, CD_3OD) δ 8.23 (d, J = 2.2 Hz, 2H), 7.67 (dd, J = 8.6, 2.3 Hz, 2H), 7.51–7.36 (m, 5H), 6.87 (d, J = 8.6 Hz, 2H), 6.59 (d, J = 3.2 Hz, 2H), 6.49 (d, J = 3.2 Hz, 2H), 3.96 (s, 4H), 3.92 (s, 2H). ^{13}C NMR (126 MHz, CD_3OD) δ 175.1 (CO), 162.5 (C), 155.9 (C), 149.5 (C), 137.4 (C), 130.8 (CH), 129.9 (CH), 129.7 (CH), 129.0 (CH), 127.1 (CH), 122.8 (C), 119.1 (C), 117.9 (CH), 114.1 (CH), 104.9 (CH), 58.2 (CH2), 52.7 (CH2). HRMS (TOF, ES$^-$): *m/z* calcd. For $C_{31}H_{24}NO_8$ (M-H^+)$^-$ 538.1502, found 538.1494 (deviation −1.5 ppm). HPLC: (λ = 254 nm): 99%; t_R = 12.61 min (λ = 214 nm): 99%; t_R = 12.61 min (HPLC method 2).

4.2.3.13. Ammonium 5-{5-{N-[5-(3-carboxy-4-hydroxyphenyl)-2-furanylmethyl]-N-propargylaminomethyl}-2-furanyl}-2-hydroxybenzoate (9l). Formed during the chromatographic purification of **2l**. Solid, mp 138–140 °C (decomposition). ^{1}H NMR (300 MHz, CD_3OD) δ 8.22 (d, J = 2.3 Hz, 2H), 7.70 (dd, J = 8.6, 2.4 Hz, 2H), 6.87 (d, J = 8.7 Hz, 2H), 6.57 (d, J = 3.3 Hz, 2H), 6.44 (d, J = 3.3 Hz, 2H), 3.88 (s, 4H), 3.45 (d, J = 2.5 Hz, 2H), 2.78 (s, 1H). ^{13}C NMR (126 MHz, CD_3OD) δ 175.3, 169.3, 162.9, 157.2, 132.3, 129.7, 127.4, 122.0, 117.8, 114.8, 104.9, 78.0, 69.1, 43.9, 36.7. HRMS (TOF, ES$^-$): *m/z* calcd. For $C_{27}H_{20}NO_8$ (M-H^+)$^-$ 486.1189, found 486.1193 (deviation +0.8 ppm). HPLC: (λ = 254 nm): 100%; t_R = 13.06 min (λ = 214 nm): 96%; t_R = 13.06 min (HPLC method 2).

4.2.3.14. Triethylammonium 5-{5-{[N-benzyl-N-(furan-2-ylmethyl) amino]methyl}furan-2-yl}-2-hydroxybenzoate (11). Reductive amination general procedure, **2f** (30 mg, 0.088 mmol), 2-furaldehyde (11 μL, 0.132 mmol), sodium triacetoxyborohydride (37 mg, 0.176 mmol), DCM (3 mL), MeOH (1 mL). Imine formation, 24 h; reduction, 3 h. Purification: Gradient elution using AcOEt/ACN/MeOH 70:10:5 → 70:10:10. Yield: 40% (18 mg, 0.036 mmol) (yellow solid). ^{1}H NMR (500 MHz, CD_3OD) δ 8.23 (d, J = 2.2 Hz, 1H), 7.67 (dd, J = 8.5, 2.3 Hz, 1H), 7.54 (s, 1H), 7.44 (d, J = 7.1 Hz, 2H), 7.37 (t, J = 7.5 Hz, 2H), 7.30 (t, J = 7.3 Hz, 1H), 6.88 (d, J = 8.6 Hz, 1H), 6.58 (d, J = 3.2 Hz, 1H), 6.43 (s, 3H), 3.85 (d, J = 7.7 Hz, 4H), 3.81 (s, 2H), 3.21 (q, J = 7.3 Hz, 6H), 1.31 (t, J = 7.3 Hz, 9H). ^{13}C NMR (126 MHz, CD_3OD) δ 175.0 (CO), 162.4 (C), 155.6 (C), 150.1 (C), 144.0 (CH), 138.1 (C), 130.6 (CH), 130.2 (C), 130.0 (CH), 129.5 (CH), 128.8 (CH), 127.0 (CH), 122.9 (C), 118.8 (C), 117.9 (CH), 113.5 (CH), 111.46 (CH), 111.42 (CH), 104.8 (CH), 58.2 (CH2), 50.1 (CH2), 50.0 (CH2), 49.7 (3CH2), 9.2 (3CH3). HRMS (TOF, ES$^+$): *m/z* calcd. For $C_{24}H_{22}NO_5$ (M + H^+)$^+$ 404.1498, found 404.1504 (deviation +1.5 ppm). HPLC: (λ = 254 nm): 98%; t_R = 11.16 min (λ = 214 nm): 99%; t_R = 11.16 min (HPLC method 2).

4.3. Biological methods

4.3.1. Production and purification of enzymes hGO and mGO

BL21 (DE3) *E. coli* transformed with recombinant pET-15 b expression vector carrying the coding sequence of mouse *Hao1* cDNA and an N-terminal His-tag was grown in the presence of 0.1 mg/mL ampicillin in LB medium for 3 h at 37 °C. The expression was induced with the addition of 0.5 mM IPTG (isopropyl β-D-thiogalactopyranoside), followed by incubation for 5 h at 25 °C. Bacteria were split in aliquots, centrifuged at 4500 g for 10 min at 4 °C (Kokusan H-251 centrifuge) and resuspended in phosphate-buffered saline (20 mM NaH_2PO_4, 500 mM NaCl, pH 7.5). After that, bacteria were re-centrifuged (Hettich Universal 320 R centrifuge) at 2800 g for 10 min at 4 °C and the pellets were frozen at −80 °C overnight. The following day cells were thawed, resuspended in cold lysis buffer (20 mM NaH_2PO_4, 500 mM NaCl, 20 mM imidazole, 50 μM FMN, pH 7.5) in the presence of PMSF (protease inhibitor) and sonicated. The samples were then centrifuged at 15 000 rpm for 10 min at 4 °C and the enzyme contained within the supernatant was purified by immobilized metal affinity chromatography (IMAC). To this end, the soluble fraction was loaded into a His GraviTrap™ column (GE-Heathcare) in order to bind the His-tagged protein to the Ni Sepharose® stationary phase. This fraction (pre-column fraction) was then eluted and the column was washed with three bed volumes of lysis-binding-wash buffer to remove unbound proteins (wash fraction). Then, elution buffer (20 mM NaH_2PO_4, 500 mM NaCl, 300 mM imidazole, pH 7.5) was added to the column and GO was eluted in two fractions of 500 μL (F1) and 2500 μL (F2). F2 was subjected to buffer exchange using a PD-10 desalting column containing Sephadex™ G-25 resin (GE-Heathcare). For that, 2500 μL corresponding to F2 were loaded into the column and eluted in 3.2 mL of working buffer (20 mM NaH_2PO_4, 500 mM NaCl, pH 7.5). Finally, the protein concentration was measured spectrophotometrically according to the extinction molar coefficient of $\mathcal{E}280$ = 48 000 M^{-1} cm^{-1} corresponding to the primary sequence of the enzyme. The enzyme was split in aliquots, preserved in liquid nitrogen and stored at −80 °C.

For the obtainment of *h*GO the same procedure was repeated using the recombinant pET-15 b expression vector carrying the coding sequence of human *Hao1* cDNA.

4.3.2. Method for the determination of the inhibition percentage against recombinant GO using an end-point fluorometric protocol [64]

Compounds were tested at 20 μM in OptiPlate black opaque 96-well microplates (PerkinElmer). In each plate, three replicates of a control for 100% enzymatic activity were included (containing substrate but not inhibitor) along with three/four replicates of each tested inhibitor at 20 μM. The reaction mixture in the wells (200 μL/well) was composed of 50 mM phosphate buffer pH 7, GO (25 nM), glycolate (180 μM), Amplex® Red (50 μM), HRP (5 units) and a solution of the inhibitor at the corresponding concentration in DMSO or just DMSO in the 100% activity control wells.

Protocol: In each well, 38 μL of 50 mM phosphate buffer pH 7 were

added. The inhibitors were then added (2 μL in DMSO) in each sample well or the same volume of DMSO in the case of the 100% control wells. Later, GO (10 μL of a solution 500 nM in phosphate buffer) was added to each well and the mixture was incubated for 10 min at rt. After this time, 50 μL of glycolate (solution 720 μM in water) were added and the mixture is incubated for 10 min at rt. After this incubation time, 100 μL of a mixture Amplex® Red/HRP (composed by Amplex® Red 100 μM and HRP (2 units/40 μL of mixture) were added and the final mixture was incubated for 10 min more at rt and in darkness. Finally, fluorescence was read at λ_{ex} 560 ± 10 nm and λ_{em} 590 ± 10 nm (PerkinElmer Multimode Plate Reader Enspire). The resulting signal was compared to the one obtained for the 100% activity control.

The mixture Amplex® Red/HRP was prepared by dissolution of HRP in water and addition of Amplex® Red (from a stock 10 mM in DMSO) (final concentrations in the mixture HRP = 2 units/40 μL and Amplex® Red = 100 μM).

4.3.3. Method for the determination of IC_{50} against recombinant GO using an end-point fluorometric protocol

The same protocol described for the determination of the inhibition percentages was followed. In this case, the inhibitor was added to each well by serial dilution, considering that all the wells will contain 40 μL (inhibitor in DMSO + phosphate buffer) before the addition of GO and that the final volume of DMSO in each well must be of 2 μL maximum (wells with the highest concentration of inhibitor).

4.3.4. Method for the determination of the inhibition percentage against recombinant LDH using a kinetic fluorometric protocol [29,65]

Compounds were tested at 10 μM in OptiPlate black opaque 96-well microplates (PerkinElmer). In each plate, along with four replicates per inhibitor to test at 10 μM, four replicates of the following control wells were included: 0% enzymatic activity (no substrate and no inhibitor), 100% enzymatic activity (with substrate but without inhibitor). The reaction mixture in the wells (200 μL/well) was composed of 50 mM phosphate buffer pH 7 (35 μL), a solution of the inhibitor in DMSO (final concentration 10 μM) or just DMSO in the control wells, LDH (Novusbio NBP1-40407 and NBP1-45281; final concentration 0.0150 U/mL), NADH (50 μL of a solution prepared at 600 μM in phosphate buffer, for a final concentration of 150 μM in the well), pyruvate (final concentration of 1 mM) or just 100 μL of phosphate buffer in the 0% activity control well.

In the control wells 1 and 2, the appropriate amounts of phosphate buffer and DMSO were added. In the wells corresponding to inhibitors, 5 μL of the solution containing the inhibitor in DMSO were added on 35 μL of phosphate buffer. At this point, 60 μL of a mixture containing LDH and NADH were added to each well. This mixture was prepared by dissolution of NADH in 50 μL of phosphate buffer (600 μM) and addition of 10 μL of a solution containing LDH in phosphate buffer (0.3 U/mL). The mixture of NADH and LDH must be prepared in darkness and the protocol must be continued in darkness from this moment. The plates were then incubated at rt during 10 min, during which the baseline was read at λ_{ex} 340 nm and λ_{em} 460 nm every 60 s (PerkinElmer Multimode Plate Reader Enspire instrument). Afterwards, the solution of substrate (2 mM pyruvate in phosphate buffer) was added to each well (100 μL/well), except for the 0% activity control in which 100 μL of phosphate buffer were added. The plate was immediately introduced in the reader instrument and fluorescence was registered at λ_{ex} 340 nm y λ_{em} 460 nm every 60 s during 10 min. The 10 min linear interval was used for slope calculation. This slope was corrected with the baseline reading registered before the addition of the substrate. The resulting corrected slope was compared to the one obtained for the 100% activity control.

4.3.5. Method for the determination of IC_{50} against recombinant LDH using a kinetic fluorometric protocol

The same protocol described for the determination of the inhibition percentages was followed. In this case, the inhibitor was added to each well by serial dilution, considering that all the wells will contain 40 μL (inhibitor in DMSO + phosphate buffer) before the addition of LDH/NADH and that the final volume of DMSO in each well must be of 2 μL maximum (wells with the highest concentration of inhibitor).

In this case, the reaction mixture in the wells (200 μL/well) was composed of 50 mM phosphate buffer pH 7 (38 μL), a solution of the inhibitor in DMSO (2 μL) or just DMSO (2 μL) in the control wells, LDH (10 μL of a stock in phosphate buffer of 0.3 U/mL, for a final concentration of 0.015 U/mL in the well), NADH (50 μL of a solution prepared at 600 μM in phosphate buffer, for a final concentration of 150 μM in the well), pyruvate (100 μL of a solution prepared at 2 mM in phosphate buffer) (for a final concentration of 1 mM in the well) or just 100 μL of phosphate buffer in the 0% activity control well.

4.3.6. Method for the determination of inhibition kinetics on GO using a kinetic fluorometric protocol [64]

For each K_i determination, three replicates of four/five different concentrations of the inhibitor in the presence of ten substrate concentrations were included. The reaction mixture in the wells (200 μL/well) was composed of 50 mM phosphate buffer pH 7 (35 μL), a solution of the inhibitor at the corresponding concentration in DMSO (5 μL), GO (10 μL of a solution 500 nM in phosphate buffer, for a final concentration of 25 nM in the well), glycolate (50 μL of a solution in water at the corresponding concentration), 100 μL of a mixture containing Amplex® Red 100 μM and 5 units of HRP in water (2 units/40 μL of the mixture) (for a final concentration of Amplex® Red of 50 μM in the well; the Amplex® Red reagent is added to the mixture from a stock 10 mM prepared in DMSO).

In each well, the corresponding amount of buffer phosphate was added (35 μL). The inhibitor was then added at the corresponding concentration in DMSO (5 μL) or the same volume of DMSO in the case of K_M determination. Later, 10 μL of 500 nM GO were added to each well. Immediately, 100 μL of the Amplex® Red/HRP mixture were added. This mixture must be prepared and handled in darkness. From this moment, the experiment must be completed in darkness. Right afterwards, 50 μL of glycolate at the corresponding concentration were added in each well. After the addition of glycolate, the fluorescence was read at λ_{ex} 560 ± 10 nm and λ_{em} 590 ± 10 nm (PerkinElmer Multimode Plate Reader Enspire). Each well was read every 60 s, over a period of 15 min. The 10 min linear interval was used for slope calculation. The initial velocity (v_0) was determined as the slope calculated in the linear interval of the "product *vs* time" graph representing the progression of the enzymatic reaction at each inhibitor and substrate concentration. This linear interval was observed to be of 10 min after a total measuring time of 15 min. Values of v_0 were obtained as a mean of three replicates.

4.3.7. Method for the determination of inhibition kinetics on LDH using a kinetic fluorometric protocol [29,65]

For each K_i determination, three replicates of four/five different concentrations of the inhibitor in the presence of nine/ten substrate concentrations were included. The reaction mixture in the wells (200 μL/well) was composed of 50 mM phosphate buffer pH 7, a solution of the inhibitor in DMSO, LDH (final concentration 0.0150 U/mL), NADH (final concentration 150 μM), pyruvate (final concentration 1 mM).

In each well, 35 μL of buffer phosphate were added. The inhibitor was then added at the corresponding concentration in DMSO (5 μL) or the same volume of DMSO in the case of K_M determination. At this point, 60 μL of a mixture containing LDH and NADH were added to each well. This mixture was prepared right before, by dissolution of NADH in 50 μL of phosphate buffer (600 μM) and addition of 10 μL of a solution containing LDH in phosphate buffer (0.3 U/mL). The mixture of NADH and LDH must be prepared in darkness and the protocol must continue in darkness from this moment. The plates were then incubated at rt during 10 min, during which the baseline was read at λ_{ex} 340 nm and λ_{em} 460 nm every 60 s (PerkinElmer Multimode Plate Reader Enspire instrument). Afterwards, the solution of substrate at the corresponding

concentration was added to each well (100 μL/well). The plate was immediately introduced in the reader instrument and fluorescence was registered at λ_{ex} 340 nm y λ_{em} 460 nm every 60 s during 10 min. The 10 min linear interval was used for slope calculation. This slope was corrected with the baseline reading registered before the addition of the substrate. The initial velocity (v_0) was determined as the slope calculated in the linear interval of the "product *vs* time" graph representing the progression of the enzymatic reaction at each inhibitor and substrate concentration. This linear interval was observed to be of 10 min after a total measuring time of 15 min. Values of v_0 were obtained as a mean of three replicates.

4.3.8. Method for the reversibility test of **2l** on hGO

Compound **2l** was tested following a kinetic fluorometric procedure. In each plate, four replicates of **2l** at 10xIC_{50} and 100xIC_{50} concentrations were included. Along with **2l**, compounds **1** and **9f** were evaluated in the same plate, at 10xIC_{50} and 100xIC_{50} concentrations (four replicates each). Four replicates of a control without inhibitor were also included in the plate.

For each of the tested inhibitors, two different vials were prepared containing mixtures of the inhibitor (at 10xIC_{50} and 100xIC_{50}) and the enzyme *h*GO (at 2.5 μM, 100x the concentration of the IC_{50} assay). For the preparation of the 10xIC_{50} vials, 10 μL of *h*GO (5 μM in phosphate buffer) and 10 μL of the inhibitor (20xIC_{50} in 50 mM phosphate buffer pH 7) were mixed. For the preparation of the 100xIC50 vials, 10 μL of *h*GO (5 μM in phosphate buffer pH 7) and 10 μL of the inhibitor (200xIC_{50} in 50 mM phosphate buffer pH 7) were mixed. For the control, another vial containing 10 μL of *h*GO (5 μM in phosphate buffer pH 7) and 10 μL of phosphate buffer pH 7 was prepared. All the vials were incubated for 30 min after which 2 μL of each vial were taken and added to wells (OptiPlate black opaque 96-well microplates) containing 198 μL of reaction buffer. The reaction buffer was composed of 48 μL of phosphate buffer, 50 μL of glycolate (solution 720 μM in water), 100 μL of a mixture containing Amplex® Red 100 μM and 5 units of HRP in water (2 units/40 μL of the mixture) (for a final concentration of Amplex® Red of 50 μM in the well; the Amplex® Red reagent is added to the mixture from a stock 10 mM prepared in DMSO). After the addition, the fluorescence was read at λ_{ex} 560 ± 10 nm and λ_{em} 590 ± 10 nm (PerkinElmer Multimode Plate Reader Enspire). Each well was read every 60 s, over a period of 15 min. The plots representing the progress of the reaction *vs* time, in the presence of each concentration of inhibitor, during the first 10 min (linear interval of the 100% enzymatic activity control), were used to calculate slopes. The slopes were used to determine activity percentages by comparison with the slope of the graph in the 100% activity control.

4.3.9. Method for the determination of the inhibition percentage against recombinant COX using a kinetic fluorometric protocol

To assess the activity of the compounds against COX-1 (ovine) and COX-2 (human) isozymes, a kinetic fluorometric protocol (10 min linear interval) using commercial kits was followed (BioVision Inhibitor Screening Kit). For the assays, OptiPlate black opaque 96-well microplates were used with a final volume of 100 μL per well and a final concentration of substrate (arachidonic acid) of 15 mM. In each plate, the following wells were included: Solvent Control wells [SC] (two replicates) containing no substrate and no inhibitor; Enzyme Control wells [EC] (four replicates) containing substrate but not inhibitor; Inhibitor Control wells [IC] (two replicates) containing the control inhibitor; Sample Screen wells [S] (three/four replicates) containing the sample inhibitor to be screened.

Manufacturer indications were followed. Volumes of 10 μL of the intermediate stocks of inhibitor were added in the [S] wells (the intermediate stocks were prepared by dissolving the inhibitors in COX assay buffer at a concentration 10x of the final concentration), 10 μL of the corresponding solvent were added in the [SC] wells and 10 μL of COX assay buffer were added to the [EC] wells. In the [IC] wells, 2 μL of control inhibitor and 8 μL of COX assay buffer were added. Then, volumes of 80 μL of Reaction Master Mix (composed of COX assay buffer 76 μL, COX probe 1 μL, diluted COX cofactor 2 μL, COX enzyme 1 μL) were added to each well, followed by volumes of 10 μL of diluted arachidonic acid (prepared by mixing 5 μL of arachidonic acid with 5 μL of NaOH and 90 μL of ddH_2O). The plate was introduced in the reader instrument and fluorescence was read every 60 s, over a period of 10 min, at 25 °C (λ_{ex} = 535 nm, λ_{em} 587 nm).

4.3.10. Method for the determination of the IC_{50} against recombinant COX using a kinetic fluorometric protocol

To assess IC_{50} values, the same commercial kits and protocols were used as described above. Inhibitors were tested at eight different concentrations and two/three replicates of each concentration were included in each assay.

4.3.11. Mouse hepatocytes isolation and culture

Hepatocytes were isolated by *in situ* collagenase perfusion method from male C57BL/6 *Agxt1*$^{-/-}$ *Grhpr*$^{-/-}$ and *Hoga1*$^{-/-}$ mouse livers. Culture of primary hepatocytes was performed as described previously [3]. Briefly, 3.0x10^5 cells/well were cultured in 6-well plates with Williams E medium supplemented with 5% fetal bovine serum, 2 mM L-glutamine, 100 U/mL penicillin, 100 μg/mL streptomycin, 2.2 mUI/mL insulin and 0.3 μg/mL hydrocortisone. After 6 h, medium was changed to Williams E complete medium (Biochrom, Cambridge, UK) without serum and cells were treated with compounds in the presence of 5 mM glycolate, 10 mM glycolate and 10 mM hydroxyproline for *Agxt1*$^{-/-}$, *Grhpr*$^{-/-}$ and *Hoga1*$^{-/-}$ primary hepatocytes culture, respectively. Culture medium was harvested at 24 h after treatment for oxalate quantification on secondary assays, and also at 48 h for full dose-response curves.

4.3.12. Cell viability and cytotoxicity

96-Well plates were seeded with 1.0x10^4 cells/well and treated with the same concentrations of compounds as in 6-well plates. At each time point, 20 μL of Cell Titer 96® Aqueous One Solution Reagent (Promega, Madison, WI) was added to the medium, incubated 2 h at 37 °C 5% CO_2 and measured at 490 nm. Relative cellular viability at each concentration of one inhibitor was calculated from the concentration of coloured MTS formazan found in wells treated with the inhibitor by comparison with the concentration of formazan found in wells devoid of inhibitor (negative controls).

Each relative cellular viability value at each inhibitor concentration was calculated as a media of three/four replicates.

4.3.13. Oxalate determination

Determination of oxalate excreted to the medium and urine oxalate was measured by the oxalate oxidase assay using a commercial kit (Trinity Biotech, Co Wicklow, Ireland), following manufacturer's instructions. The method involves oxidation of oxalate (1 equiv) by oxalate oxidase with formation of H_2O_2 (1 equiv) and subsequent utilization of the generated H_2O_2 for the formation of a dye (absorbance at 590 nm) in a HRP catalyzed reaction with the substrates 3-methyl-2-benzothiazolinone hydrazone (MBTH) and 3-(dimethylamino)benzoic acid (DMAB). For oxalate quantification, a standard curve was built using aqueous dilutions of oxalate containing 0, 0.025, 0.05, 0.1, 0.2 and 0.25 nmol oxalate/μL. For the standard curve, absorbance was measured at 590 nm following the same protocol described above.

For *in vitro* studies, relative oxalate for each inhibitor at the suitable concentration was calculated from the concentration of extracellular oxalate found in wells treated with the inhibitor, as a percentage of the extracellular oxalate found in wells devoid of inhibitor (negative controls). Each relative oxalate value at each inhibitor concentration was calculated as a media of three/four replicates.

For EC_{50} calculation, each inhibitor was tested at eight different concentrations. At each concentration, three/four replicates of relative

oxalate were determined. The final EC_{50} was calculated as a mean of the three/four replicates.

For *in vivo* studies, the amount of urine oxalate was normalized with the creatinine excretion (ratio oxalate/creatinine μg/mg) and expressed as relative normalized oxalate excretion referred to the control pre-treated mice (100%).

4.3.14. Urine glycolate determination

Measurements of glycolate levels in urine samples was performed with the same enzymatic assay of glycolate oxidase described above, but using 2 μg of purified protein per sample.

4.3.15. Urine creatinine determination

Urine creatinine was measured using a standard creatinine detection kit (Enzo Life Sciences, Lausen, Switzerland).

4.3.16. Administration of compound **2l** and urine collection

Animal experiments and animal care procedures were approved by the local animal ethics committee (CEIBA) and were performed in accordance with the institutional guidelines that comply with the national and international laws and policies (EEC Council Directive 86/609, OJ L 358, December 12, 1987) and with the ARRIVE guidelines (Animals in Research Reporting In Vivo Experiments). *Agxt1*$^{-/-}$ mice were placed in metabolic cages for a single mouse (Tecniplast, Buguggiate, Italy) and allowed to get acclimatized for 3 days before the start of urine collection. Eight consecutive 24-h urine collections were performed for basal urine oxalate, glycolate and creatinine determination. Next, **2l** was administered by oral gavage (in solution with 0.5% methylcellulose) at a daily dose of 20 mg/kg body weight during 5 days. All 24-h urine collections were obtained in tubes containing 50 μL of 6 M HCl. Samples with less than 1 mL urine or with food or fecal contaminations were excluded from the study.

4.3.17. Statistical analysis of in vivo experiments

Data are expressed as a mean ± standard error. Paired-sample *t*-test was used to compare pre-treated mice (control) and treated mice. All data were analyzed using IBM SPSS 20 statistical package.

4.3.18. Method for the determination of the anti-inflammatory activity in vitro

To determine *in vitro* anti-inflammatory capacity, a human monocyte model, THP-1 (ATCC® TIB-202 ™), treated with LPS (*E. coli* lipopolysaccharide) was used. Briefly, THP-1 cells were seeded in 12-well plates at 350.000 cells per well in cell culture medium (RPMI) with 2% FBS. Compounds were added to cells in an increasing dose curve and cells were incubated for 24h. Then, the induction of inflammatory response was triggered by 80 ng/mL LPS for 24h. After that, the culture supernatants are kept at −80 °C until the cytokines IL-6, IL-1β and TNF-α were measured by ELISA (Enzyme-Linked ImmunoSorbent Assay).

The cytotoxicity of each compound was analyzed by the colorimetric CCK-8 test (Cell Counting Kit-8).

ELISA kits were used to quantify IL-6 (Human IL-6 ELISA Ready-SET-Go! eBiosciences), IL-1β (Human IL-1β ELISA Set, BD Biosciences), and TNF-α (Human TNF ELISA Set, BD Biosciences), following the manufacturer's instructions. IC_{50} of each compound was calculated using *GeneData Screener Software*.

4.3.19. Method for the determination of renal cytotoxicity

Cytotoxicity tests were developed on kidney-derived lines (HEK-293, ECACC 85120602 and 786-O, ATCC CRL-1932™) by measuring cellular toxicity using the MTT metabolic test. Briefly, cells were seeded at a density of 40.000/well in a 96-wells plate and were incubated in a humidified atmosphere at 37 °C with 5% CO_2 for 24h. The compounds were dissolved in DMSO at 10 mM and the highest concentration assayed was 100 μM in 786-O and 50 μM in HEK-293. After 48 h of treatment, plates were treated with MTT [3-(4,5-dimethylthiazol-2-yl)-2,5-diphenyltetrazolium bromide] at 5 μg/mL in Minimum Essential Medium Eagle (MEM) for 2 h. Then, DMSO was added to the plates to dissolve the formazan crystals formed in viable cells and plates were stirred for 5 min to homogenize the solution. Absorbance at 570 nm was measured by VICTOR Multilabel Plate Reader (PerkinElmer). LC_{50} and Z-factor calculations were done using *GeneData Screener Software*.

4.4. Docking methods

4.4.1. Homology modeling

Homology models were constructed using MODELLER 9.23 [66] with PDB ID 1AL7 as a template of the protein and the protein sequence of *h*GO downloaded from UNIPROT [67]. A total of 100 model were obtained and classified according to its DOPE score (Table S165). The best 5 models were analyzed and their stereochemical quality and accuracy were tested using PROCHECK [68]. Results from PROCHECK reported as Ramachandran plots showed that all selected models have ≥90% of its residues in the most favoured regions A, B and L of the Ramachandran plot (results not shown). Of the 5 selected model the best in terms of DOPE score was selected for docking analysis.

4.4.2. Docking protocol

Docking studies were carried out with Autodock 4.2.6 (AD4) [69] on the crystal structures of human lactate dehydrogenase M and H isozymes forms (*h*LDHA PDB ID: 1I10; 4L4S and 6SBU; *h*LDHB PDB ID: 1I0Z) [53], and *h*GO (PDB ID: 2RDT and 2RDU). Ligands structures were built on Avogadro [70] and optimized using Gaussian (HF/6-31G d,p). Compounds presenting tertiary amines, prone to protonation at physiological pH, were also considered. Once optimized, ligands PDBs were prepared for docking using the prepare_ligand4. py script included MGLTools 1.5.4 [71]. Protein structures, on the other hand, were prepared for docking using the PDB2PQR tools [72]. Water and ligand molecules were removed and charges and non-polar hydrogen atoms were added at pH 7.0. The produced structures were saved as pdb files and prepared for docking using the prepare_receptor4. py script from MGLTools. AD4 was used to automatically dock the ligands into the *h*LDH and *h*GO binding sites. For *h*LDHA (PDB ID 1I10 and 4L4S) and *h*LDHB (PDB ID 1I0Z) the docking grid was centred on the pyruvate-NADH binding site, and set with the grid parameters 60 Å × 80 Å × 60 Å with 0.375 Å spacing. On the other hand, for *h*LDHA (PDB ID 6SBU) [46], the docking grid was centred on the cognate ligands binding site within the A and B subunits, with the grid parameters 60 Å × 60 Å × 80 Å with 0.375 Å spacing. For *h*GO (PDB ID: 2RDT, 2RDU, 1AL7-homology-model) the docking grid was centred on the FMN-CDST binding site, and set with the grid parameters 65 Å × 60 Å × 60 Å with 0.375 Å spacing. In all calculations, AD4 parameter file was set to 100 GA runs, 2.500.000 energy evaluations and a population size of 150. The Lamarckian genetic algorithm local search (GALS) method was used for the docking calculations. All dockings were performed with a population size of 250 and a Solis and Wets local search of 300 rounds was applied with a probability of 0.06. A mutation rate of 0.02 and a crossover rate of 0.8 were used. The docking results from each of the 100 calculations were clustered based on root-mean square deviation (RMSD) (solutions differing by less than 2.0 Å) between the Cartesian coordinates of the atoms, and were ranked on the basis of free energy of binding.

Chimera 1.15 was used for molecules visualization and figures generation [73].

Author contributions

All authors have given approval to the final version of the manuscript. M. D.M.G. was involved in the synthetic chemistry and the biological evaluation of the compounds on recombinant enzymes. B.R.R., C. M.H. and M.X.F. were involved in the preparation of the primary hepatocyte cultures and the biological evaluation on hepatocyte cultures and *in vivo*. F.F.M. was involved in the docking studies. A.L.P. was

involved in the production and purification of recombinant enzymes for compound screening. J.A.G., E.S. and M.D.G. were involved in the coordination and direction of the overall program and the elaboration of the manuscript.

Declaration of competing interest

The authors declare that they have no known competing financial interests or personal relationships that could have appeared to influence the work reported in this paper.

Acknowledgments

Funding: This work was supported by the Oxalosis and Hyperoxaluria Foundation (OHF) [Research Grant OHF2012], the Spanish Ministry of Economy [Predoctoral Fellowship to C.M.H. BES-2012-052719], the ERDF/Spanish Ministry of Science, Innovation and Universities [Research Projects RTI2018-098560-B-C21 and RTI2018-096246-B-I00 to M.D.G. and A.L.P, respectively], the University of Granada [Predoctoral Fellowship to M. D.M.G, Postdoctoral Grant to M. D.M.G], and the Consejería de Economía, Conocimiento, Empresas y Universidad, Junta de Andalucía [Grant P18-RT-2413 to A.L.P].

Appendix A. Supplementary data

Supplementary data to this article can be found online at https://doi.org/10.1016/j.ejmech.2022.114396.

References

[1] M.D. Moya-Garzón, C. Martín Higueras, P. Peñalver, M. Romera, M.X. Fernandes, F. Franco-Montalbán, J.A. Gómez-Vidal, E. Salido, M. Díaz-Gavilán, Salicylic acid derivatives inhibit oxalate production in mouse hepatocytes with primary hyperoxaluria type 1, J. Med. Chem. 61 (2018) 7144–7167, https://doi.org/10.1021/acs.jmedchem.8b00399.

[2] X. Zhang, S.M. Roe, Y. Hou, M. Bartlam, Z. Rao, L.H. Pearl, C.J. Danpure, Crystal structure of alanine:glyoxylate aminotransferase and the relationship between genotype and enzymatic phenotype in primary hyperoxaluria type 1, J. Mol. Biol. 331 (2003) 643–652.

[3] C. Martin-Higueras, S. Luis-Lima, E. Salido, Glycolate oxidase is a safe and efficient target for substrate reduction therapy in a mouse model of primary hyperoxaluria type I, Mol. Ther. 24 (2016) 719–725, https://doi.org/10.1038/mt.2015.224.

[4] D.P. Cregeen, E.L. Williams, S. Hulton, G. Rumsby, Molecular analysis of the glyoxylate reductase (GRHPR) gene and description of mutations underlying primary hyperoxaluria type 2, Hum. Mutat. 22 (2003), https://doi.org/10.1002/humu.9200, 497–497.

[5] R. Belostotsky, E. Seboun, G.H. Idelson, D.S. Milliner, R. Becker-Cohen, C. Rinat, C. G. Monico, S. Feinstein, E. Ben-Shalom, D. Magen, I. Weissman, C. Charon, Y. Frishberg, Mutations in DHDPSL are responsible for primary hyperoxaluria type III, Am. J. Hum. Genet. 87 (2010) 392–399, https://doi.org/10.1016/j.ajhg.2010.07.023.

[6] S.F. Garrelfs, G. Rumsby, H. Peters-Sengers, F. Erger, J.W. Groothoff, B.B. Beck, M. J.S. Oosterveld, A. Pelle, T. Neuhaus, B. Adams, P. Cochat, E. Salido, G.W. Lipkin, B. Hoppe, S.-A. Hulton, Patients with primary hyperoxaluria type 2 have significant morbidity and require careful follow-up, Kidney Int. (2019), https://doi.org/10.1016/j.kint.2019.08.018.

[7] S. M'dimegh, C. Aquaviva-Bourdain, A. Omezzine, G. Souche, I. M'barek, K. Abidi, T. Gargah, S. Abroug, A. Bouslama, HOGA1 gene mutations of primary hyperoxaluria type 3 in Tunisian patients, J. Clin. Lab. Anal. 31 (2017), https://doi.org/10.1002/jcla.22053.

[8] E. Richard, J.-M. Blouin, J. Harambat, B. Llanas, S. Bouchet, C. Acquaviva, R. de la Faille, Late diagnosis of primary hyperoxaluria type III, Ann. Clin. Biochem. 54 (2017) 406–411, https://doi.org/10.1177/0004563216677101.

[9] C. Martin-Higueras, S.F. Garrelfs, J.W. Groothoff, D. Jacob, S.H. Moochhala, J. Bacchetta, C. Acquaviva, M. Zaniew, P. Sikora, B.B. Beck, B. Hoppe, A report from the European Hyperoxaluria Consortium (OxalEurope) Registry on a large cohort of patients with primary hyperoxaluria type 3, Kidney Int. (2021), https://doi.org/10.1016/j.kint.2021.03.031.

[10] P. Singh, J.K. Viehman, R.A. Mehta, A.G. Cogal, L. Hasadsri, D. Oglesbee, J. B. Olson, B.M. Seide, D.J. Sas, P.C. Harris, J.C. Lieske, D.S. Milliner, Clinical characterization of primary hyperoxaluria type 3 in comparison to types 1 and 2: a retrospective cohort study, Nephrol. Dial. Transplant. (2021), https://doi.org/10.1093/ndt/gfab027.

[11] C.G. Monico, S. Rossetti, J.B. Olson, D.S. Milliner, Pyridoxine effect in type I primary hyperoxaluria is associated with the most common mutant allele, Kidney Int. 67 (2005) 1704–1709, https://doi.org/10.1111/j.1523-1755.2005.00267.x.

[12] S. Fargue, G. Rumsby, C.J. Danpure, Multiple mechanisms of action of pyridoxine in primary hyperoxaluria type 1, Biochim. Biophys. Acta (BBA) - Mol. Basis Dis. 1832 (2013) 1776–1783, https://doi.org/10.1016/j.bbadis.2013.04.010.

[13] E. Salido, A.L. Pey, R. Rodriguez, V. Lorenzo, Primary hyperoxalurias: disorders of glyoxylate detoxification, Biochim. Biophys. Acta (BBA) - Mol. Basis Dis. 1822 (2012) 1453–1464, https://doi.org/10.1016/j.bbadis.2012.03.004.

[14] P. Cochat, G. Rumsby, Primary hyperoxaluria, N. Engl. J. Med. 369 (2013) 649–658, https://doi.org/10.1056/NEJMra1301564.

[15] M. Dindo, S. Grottelli, G. Annunziato, G. Giardina, M. Pieroni, G. Pampalone, A. Faccini, F. Cutruzzolà, P. Laurino, G. Costantino, B. Cellini, Cycloserine enantiomers are reversible inhibitors of human alanine:glyoxylate aminotransferase: implications for Primary Hyperoxaluria type 1, Biochem. J. 476 (2019) 3751–3768, https://doi.org/10.1042/BCJ20190507.

[16] B. Buchalski, K.D. Wood, A. Challa, S. Fargue, R.P. Holmes, W.T. Lowther, J. Knight, The effects of the inactivation of Hydroxyproline dehydrogenase on urinary oxalate and glycolate excretion in mouse models of primary hyperoxaluria, Biochim. Biophys. Acta (BBA) - Mol. Basis Dis. 1866 (2020) 165633, https://doi.org/10.1016/j.bbadis.2019.165633.

[17] A. Weigert, C. Martin-Higueras, B. Hoppe, Novel therapeutic approaches in primary hyperoxaluria, Expet Opin. Emerg. Drugs 23 (2018) 349–357, https://doi.org/10.1080/14728214.2018.1552940.

[18] R. Belostotsky, Y. Frishberg, Novel therapeutic approaches for the primary hyperoxalurias, Pediatr. Nephrol. (2020), https://doi.org/10.1007/s00467-020-04817-8.

[19] L.J. Scott, S.J. Keam, Lumasiran: first approval, Drugs 81 (2021) 277–282, https://doi.org/10.1007/s40265-020-01463-0.

[20] S.F. Garrelfs, Y. Frishberg, S.A. Hulton, M.J. Koren, W.D. O'Riordan, P. Cochat, G. Deschênes, H. Shasha-Lavsky, J.M. Saland, W.G. van't Hoff, D.G. Fuster, D. Magen, S.H. Moochhala, G. Schalk, E. Simkova, J.W. Groothoff, D.J. Sas, K. A. Meliambro, J. Lu, M.T. Sweetser, P.P. Garg, A.K. Vaishnaw, J.M. Gansner, T. L. McGregor, J.C. Lieske, Lumasiran, an RNAi therapeutic for primary hyperoxaluria type 1, N. Engl. J. Med. 384 (2021) 1216–1226, https://doi.org/10.1056/NEJMoa2021712.

[21] D. Erbe, Methods for Inhibition of Hao1 (Hydroxyacid Oxidase 1 (Glycolate Oxidase) Gene Expression, WO2019014491A1, 2019.

[22] K. Garber, Alnylam launches era of RNAi drugs, Nat. Biotechnol. 36 (2018) 777–778, https://doi.org/10.1038/nbt0918-777.

[23] C. Lai, N. Pursell, J. Gierut, U. Saxena, W. Zhou, M. Dills, R. Diwanji, C. Dutta, M. Koser, N. Nazef, R. Storr, B. Kim, C. Martin-Higueras, E. Salido, W. Wang, M. Abrams, H. Dudek, B.D. Brown, Specific inhibition of hepatic lactate dehydrogenase reduces oxalate production in mouse models of primary hyperoxaluria, Mol. Ther. 26 (2018) 1983–1995, https://doi.org/10.1016/j.ymthe.2018.05.016.

[24] G. Ariceta, K. Barrios, B.D. Brown, B. Hoppe, R. Rosskamp, C.B. Langman, Hepatic lactate dehydrogenase A: an RNA interference target for the treatment of all known types of primary hyperoxaluria, Kidney Int Rep 6 (2021) 1088–1098, https://doi.org/10.1016/j.ekir.2021.01.029.

[25] B. Hoppe, A. Koch, P. Cochat, S.F. Garrelfs, M.A. Baum, J.W. Groothoff, G. Lipkin, M. Coenen, G. Schalk, A. Amrite, D. McDougall, K. Barrios, C.B. Langman, Safety, pharmacodynamics, and exposure-response modeling results from a first in human phase 1 study of nedosiran in primary hyperoxaluria, Kidney Int. (21) (2021) S0085–S2538, https://doi.org/10.1016/j.kint.2021.08.015, 00807–3.

[26] M.L. Dudal, L. Huguet, J. Perez, S. Vandermeersch, E. Bouderlique, E. Tang, C. Martori, N. Chemaly, R. Nabbout, J.-P. Haymann, V. Frochot, L. Baud, G. Deschênes, M. Daudon, E. Letavernier, Stiripentol protects against calcium oxalate nephrolithiasis and ethylene glycol poisoning, J. Clin. Invest. 129 (2019) 2571–2577, https://doi.org/10.1172/JCI99822.

[27] C. Kempf, A. Pfau, J. Holle, K. Müller-Schlüter, P. Bufler, F. Knauf, D. Müller, Stiripentol fails to lower plasma oxalate in a dialysis-dependent PH1 patient, Pediatr. Nephrol. 35 (2020) 1787–1789, https://doi.org/10.1007/s00467-020-04585-5.

[28] E. Letavernier, M. Daudon, Stiripentol identifies a therapeutic target to reduce oxaluria, Curr. Opin. Nephrol. Hypertens. 29 (2020) 394–399, https://doi.org/10.1097/MNH.0000000000000621.

[29] S. Rupiani, R. Buonfiglio, M. Manerba, L. Di Ianni, M. Vettraino, E. Giacomini, M. Masetti, F. Falchi, G. Di Stefano, M. Roberti, M. Recanatini, Identification of N-acylhydrazone derivatives as novel lactate dehydrogenase A inhibitors, Eur. J. Med. Chem. 101 (2015) 63–70, https://doi.org/10.1016/j.ejmech.2015.06.028.

[30] J.R. Doherty, J.L. Cleveland, Targeting lactate metabolism for cancer therapeutics, J. Clin. Invest. 123 (2013) 3685–3692, https://doi.org/10.1172/JCI69741.

[31] C.L. Markert, J.B. Shaklee, G.S. Whitt, Evolution of a gene, Science 189 (1975) 102–114, https://doi.org/10.1126/science.1138367.

[32] J. Ding, R. Gumpena, M.-O. Boily, A. Caron, O. Chong, J.H. Cox, V. Dumais, S. Gaudreault, A.H. Graff, A. King, J. Knight, R. Oballa, J. Surendradoss, T. Tang, J. Wu, W.T. Lowther, D.A. Powell, Dual glycolate oxidase/lactate dehydrogenase A inhibitors for primary hyperoxaluria, ACS Med. Chem. Lett. 12 (2021) 1116–1123, https://doi.org/10.1021/acsmedchemlett.1c00196.

[33] M.S. Murray, R.P. Holmes, W.T. Lowther, Active site and loop 4 movements within human glycolate oxidase: implications for substrate specificity and drug design, Biochemistry 47 (2008) 2439–2449, https://doi.org/10.1021/bi701710r.

[34] W.H. Brown, B.J. Hutchinson, Intermediates in the cycloanhydrotetramerization of furan with aliphatic and alicyclic ketones, Can. J. Chem. 56 (1978) 617–621, https://doi.org/10.1139/v78-100.

[35] M. Choura, N.M. Belgacem, A. Gandini, Acid-catalyzed polycondensation of furfuryl alcohol: mechanisms of chromophore formation and cross-linking, Macromolecules 29 (1996) 3839–3850, https://doi.org/10.1021/ma951522f.

[36] R.I. Khusnutdinov, A.R. Baiguzina, A.A. Smirnov, R.R. Mukminov, U. M. Dzhemilev, Furfuryl alcohol in synthesis of levulinic acid esters and difurylmethane with Fe and Rh complexes, Russ. J. Appl. Chem. 80 (n.d.) (1687) 1690, https://doi.org/10.1134/S1070427207100163.
[37] E.R. Sacia, M. Balakrishnan, A.T. Bell, Biomass conversion to diesel via the etherification of furanyl alcohols catalyzed by Amberlyst-15, J. Catal. 313 (2014) 70–79, https://doi.org/10.1016/j.jcat.2014.02.012.
[38] T. Kim, R.S. Assary, R.E. Pauls, C.L. Marshall, L.A. Curtiss, P.C. Stair, Thermodynamics and reaction pathways of furfuryl alcohol oligomer formation, Catal. Commun. 46 (2014) 66–70, https://doi.org/10.1016/j.catcom.2013.11.030.
[39] G. Rücker, M. Neugebauer, M. Neugebauer, Zur chemischen Stabilität von Furfenorex und analogen Modellsubstanzen, Arch. Pharm. Pharm. Med. Chem. 319 (1986) 317–324, https://doi.org/10.1002/ardp.19863190406.
[40] Evaluation of Enzyme Inhibitors in Drug Discovery: A Guide for Medicinal Chemists and Pharmacologists, 2nd Edition | Wiley, Wiley.Com. (n.d.), https://www.wiley.com/en-us/Evaluation+of+Enzyme+Inhibitors+in+Drug+Discovery%3A+A+Guide+for+Medicinal+Chemists+and+Pharmacologists%2C+2nd+Edition-p-9781118488133. (Accessed 22 July 2021).
[41] A.S. Kalgutkar, N. Castagnoli, B. Testa, Selective inhibitors of monoamine oxidase (MAO-A and MAO-B) as probes of its catalytic site and mechanism, Med. Res. Rev. 15 (1995) 325–388, https://doi.org/10.1002/med.2610150406.
[42] B. Kumar, V. Kumar, V. Prashar, S. Saini, A.R. Dwivedi, B. Bajaj, D. Mehta, J. Parkash, V. Kumar, Dipropargyl substituted diphenylpyrimidines as dual inhibitors of monoamine oxidase and acetylcholinesterase, Eur. J. Med. Chem. 177 (2019) 221–234, https://doi.org/10.1016/j.ejmech.2019.05.039.
[43] K. Mdluli, M.P.S. Booth, R.L. Brady, G. Rumsby, A preliminary account of the properties of recombinant human Glyoxylate reductase (GRHPR), LDHA and LDHB with glyoxylate, and their potential roles in its metabolism, Biochim. Biophys. Acta Protein Proteonomics 1753 (2005) 209–216, https://doi.org/10.1016/j.bbapap.2005.08.004.
[44] Y. Blat, Non-competitive inhibition by active site binders, Chem. Biol. Drug Des. 75 (2010) 535–540, https://doi.org/10.1111/j.1747-0285.2010.00972.x.
[45] A.L. Shirfule, A.T. Sangamwar, C.N. Khobragade, Exploring glycolate oxidase (GOX) as an antiurolithic drug target: molecular modeling and in vitro inhibitor study, Int. J. Biol. Macromol. 49 (2011) 62–70, https://doi.org/10.1016/j.ijbiomac.2011.03.016.
[46] A. Friberg, H. Rehwinkel, D. Nguyen, V. Pütter, M. Quanz, J. Weiske, U. Eberspächer, I. Heisler, G. Langer, Structural evidence for isoform-selective allosteric inhibition of lactate dehydrogenase A, ACS Omega 5 (2020) 13034–13041, https://doi.org/10.1021/acsomega.0c00715.
[47] M.W. Dzierlenga, S.D. Schwartz, Targeting a rate-promoting vibration with an allosteric mediator in lactate dehydrogenase, J. Phys. Chem. Lett. 7 (2016) 2591–2596, https://doi.org/10.1021/acs.jpclett.6b01209.
[48] E.C. Salido, X.M. Li, Y. Lu, X. Wang, A. Santana, N. Roy-Chowdhury, A. Torres, L. J. Shapiro, J. Roy-Chowdhury, Alanine-glyoxylate aminotransferase-deficient mice, a model for primary hyperoxaluria that responds to adenoviral gene transfer, Proc. Natl. Acad. Sci. U.S.A. 103 (2006) 18249–18254, https://doi.org/10.1073/pnas.0607218103.
[49] J. Knight, R.P. Holmes, S.D. Cramer, T. Takayama, E. Salido, Hydroxyproline metabolism in mouse models of primary hyperoxaluria, Am. J. Physiol. Ren. Physiol. 302 (2012) F688–F693, https://doi.org/10.1152/ajprenal.00473.2011.
[50] X. Li, J. Knight, W.T. Lowther, R.P. Holmes, Hydroxyproline metabolism in a mouse model of primary hyperoxaluria type 3, Biochim. Biophys. Acta 1852 (2015) 2700–2705, https://doi.org/10.1016/j.bbadis.2015.09.016.
[51] K. Stenberg, Y. Lindqvist, Three-dimensional structures of glycolate oxidase with bound active-site inhibitors, Protein Sci. 6 (1997) 1009–1015, https://doi.org/10.1002/pro.5560060506.
[52] S. Dempster, S. Harper, J.E. Moses, I. Dreveny, Structural characterization of the apo form and NADH binary complex of human lactate dehydrogenase, Acta Crystallogr. D 70 (2014) 1484–1490, https://doi.org/10.1107/S1399004714005422.
[53] J.A. Read, V.J. Winter, C.M. Eszes, R.B. Sessions, R.L. Brady, Structural basis for altered activity of M- and H-isozyme forms of human lactate dehydrogenase, Protein. Struct. Funct. Bioinf. 43 (2001) 175–185, https://doi.org/10.1002/1097-0134(20010501)43:2<175::AID-PROT1029>3.0.CO;2-#.
[54] S. Labadie, P.S. Dragovich, J. Chen, B.P. Fauber, J. Boggs, L.B. Corson, C.Z. Ding, C. Eigenbrot, H. Ge, Q. Ho, K.W. Lai, S. Ma, S. Malek, D. Peterson, H.E. Purkey, K. Robarge, L. Salphati, S. Sideris, M. Ultsch, E. VanderPorten, B. Wei, Q. Xu, I. Yen, Q. Yue, H. Zhang, X. Zhang, A. Zhou, Optimization of 5-(2,6-dichlorophenyl)-3-hydroxy-2-mercaptocyclohex-2-enones as potent inhibitors of human lactate dehydrogenase, Bioorg. Med. Chem. Lett 25 (2015) 75–82, https://doi.org/10.1016/j.bmcl.2014.11.008.
[55] P.S. Dragovich, B.P. Fauber, L.B. Corson, C.Z. Ding, C. Eigenbrot, H. Ge, A. M. Giannetti, T. Hunsaker, S. Labadie, Y. Liu, S. Malek, B. Pan, D. Peterson, K. Pitts, H.E. Purkey, S. Sideris, M. Ultsch, E. VanderPorten, B. Wei, Q. Xu, I. Yen, Q. Yue, H. Zhang, X. Zhang, Identification of substituted 2-thio-6-oxo-1,6-dihydropyrimidines as inhibitors of human lactate dehydrogenase, Bioorg. Med. Chem. Lett 23 (2013) 3186–3194, https://doi.org/10.1016/j.bmcl.2013.04.001.
[56] B.P. Fauber, P.S. Dragovich, J. Chen, L.B. Corson, C.Z. Ding, C. Eigenbrot, A. M. Giannetti, T. Hunsaker, S. Labadie, Y. Liu, Y. Liu, S. Malek, D. Peterson, K. Pitts, S. Sideris, M. Ultsch, E. VanderPorten, J. Wang, B. Wei, I. Yen, Q. Yue, Identification of 2-amino-5-aryl-pyrazines as inhibitors of human lactate dehydrogenase, Bioorg. Med. Chem. Lett 23 (2013) 5533–5539, https://doi.org/10.1016/j.bmcl.2013.08.060.
[57] A. Kohlmann, S.G. Zech, F. Li, T. Zhou, R.M. Squillace, L. Commodore, M. T. Greenfield, X. Lu, D.P. Miller, W.-S. Huang, J. Qi, R.M. Thomas, Y. Wang, S. Zhang, R. Dodd, S. Liu, R. Xu, Y. Xu, J.J. Miret, V. Rivera, T. Clackson, W. C. Shakespeare, X. Zhu, D.C. Dalgarno, Fragment growing and linking lead to novel nanomolar lactate dehydrogenase inhibitors, J. Med. Chem. 56 (2013) 1023–1040, https://doi.org/10.1021/jm3014844.
[58] R.A. Ward, C. Brassington, A.L. Breeze, A. Caputo, S. Critchlow, G. Davies, L. Goodwin, G. Hassall, R. Greenwood, G.A. Holdgate, M. Mrosek, R.A. Norman, S. Pearson, J. Tart, J.A. Tucker, M. Vogtherr, D. Whittaker, J. Wingfield, J. Winter, K. Hudson, Design and synthesis of novel lactate dehydrogenase A inhibitors by fragment-based lead generation, J. Med. Chem. 55 (2012) 3285–3306, https://doi.org/10.1021/jm201734r.
[59] S. Kolappan, D.L. Shen, R. Mosi, J. Sun, E.J. McEachern, D.J. Vocadlo, L. Craig, Structures of lactate dehydrogenase A (LDHA) in apo, ternary and inhibitor-bound forms, Acta Crystallogr. D 71 (2015) 185–195, https://doi.org/10.1107/S1399004714024791.
[60] Internal Enzyme Motions as a Source of Catalytic Activity: Rate-Promoting Vibrations and Hydrogen Tunneling, J. Phys. Chem. B (n.d.), https://pubs.acs.org/doi/10.1021/jp004547b. (Accessed 28 January 2021).
[61] S.L. Quaytman, S.D. Schwartz, Reaction coordinate of an enzymatic reaction revealed by transition path sampling, Proc. Natl. Acad. Sci. U. S. A. 104 (2007) 12253–12258, https://doi.org/10.1073/pnas.0704304104.
[62] J.E. Masterson, S.D. Schwartz, Changes in protein architecture and subpicosecond protein dynamics impact the reaction catalyzed by lactate dehydrogenase, J. Phys. Chem. 117 (2013) 7107–7113, https://doi.org/10.1021/jp400376h.
[63] C.M. Salisbury, B.F. Cravatt, Activity-based probes for proteomic profiling of histone deacetylase complexes, Proc. Natl. Acad. Sci. Unit. States Am. 104 (2007) 1171–1176, https://doi.org/10.1073/pnas.0608659104.
[64] M. Wang, M. Xu, Y. Long, S. Fargue, N. Southall, X. Hu, J.C. McKew, C.J. Danpure, W. Zheng, High throughput cell-based assay for identification of glycolate oxidase inhibitors as a potential treatment for Primary Hyperoxaluria Type 1, Sci. Rep. 6 (2016) 34060, https://doi.org/10.1038/srep34060.
[65] P.S. Dragovich, B.P. Fauber, J. Boggs, J. Chen, L.B. Corson, C.Z. Ding, C. Eigenbrot, H. Ge, A.M. Giannetti, T. Hunsaker, S. Labadie, C. Li, Y. Liu, Y. Liu, S. Ma, S. Malek, D. Peterson, K.E. Pitts, H.E. Purkey, K. Robarge, L. Salphati, S. Sideris, M. Ultsch, E. VanderPorten, J. Wang, B. Wei, Q. Xu, I. Yen, Q. Yue, H. Zhang, X. Zhang, A. Zhou, Identification of substituted 3-hydroxy-2-mercaptocyclohex-2-enones as potent inhibitors of human lactate dehydrogenase, Bioorg. Med. Chem. Lett 24 (2014) 3764–3771, https://doi.org/10.1016/j.bmcl.2014.06.076.
[66] N. Eswar, B. Webb, M.A. Marti-Renom, M.S. Madhusudhan, D. Eramian, M.-Y. Shen, U. Pieper, A. Sali, Comparative protein structure modeling using Modeller (Chapter 5), Curr.Protoc.Bioinf. (2006), https://doi.org/10.1002/0471250953.bi0506s15. Unit-5.6.
[67] UniProt (n.d.), https://www.uniprot.org/. (Accessed 27 July 2021).
[68] R.A. Laskowski, M.W. MacArthur, D.S. Moss, J.M. Thornton, PROCHECK: a program to check the stereochemical quality of protein structures, J. Appl. Crystallogr. 26 (1993) 283–291, https://doi.org/10.1107/S0021889892009944.
[69] G.M. Morris, R. Huey, W. Lindstrom, M.F. Sanner, R.K. Belew, D.S. Goodsell, A. J. Olson, AutoDock 4 and AutoDockTools 4: automated docking with selective receptor flexibility, J. Comput. Chem. 30 (2009) 2785–2791, https://doi.org/10.1002/jcc.21256.
[70] M.D. Hanwell, D.E. Curtis, D.C. Lonie, T. Vandermeersch, E. Zurek, G.R. Hutchison, Avogadro: an advanced semantic chemical editor, visualization, and analysis platform, J. Cheminf. 4 (2012) 17, https://doi.org/10.1186/1758-2946-4-17.
[71] M.F. Sanner, Python: a programming language for software integration and development, J. Mol. Graph. Model. 17 (1999) 57–61.
[72] T.J. Dolinsky, P. Czodrowski, H. Li, J.E. Nielsen, J.H. Jensen, G. Klebe, N.A. Baker, PDB2PQR: expanding and upgrading automated preparation of biomolecular structures for molecular simulations, Nucleic Acids Res. 35 (2007) W522–W525, https://doi.org/10.1093/nar/gkm276.
[73] E.F. Pettersen, T.D. Goddard, C.C. Huang, G.S. Couch, D.M. Greenblatt, E.C. Meng, T.E. Ferrin, UCSF Chimera–a visualization system for exploratory research and analysis, J. Comput. Chem. 25 (2004) 1605–1612, https://doi.org/10.1002/jcc.20084.